DEPARTMENT OF PHYSICS
UNIVERSITY OF JYVÄSKYLÄ
RESEARCH REPORT No. 12/2010

THERMODYNAMICS OF TWO–FLAVOR QCD FROM CHIRAL MODELS WITH POLYAKOV LOOP

BY
TOPI KÄHÄRÄ

Academic Dissertation
for the Degree of
Doctor of Philosophy

To be presented, by permission of the
Faculty of Mathematics and Natural Sciences
of the University of Jyväskylä,
for public examination in Auditorium FYS1 of the
University of Jyväskylä on December 10th, 2010
at 12 o'clock noon

Jyväskylä, Finland
December 2010

Preface

This thesis is the result of work carried out at the Department of Physics of the University of Jyväskylä (JYFL) during the years 2006–2010 under the supervision of Docent Kimmo Tuominen. The work was funded by JYFL, The Helsinki Institute of Physics and The Väisälä Foundation through The Finnish Academy of Science and Letters.

As the author I would like to thank my supervisor Kimmo Tuominen for overseeing the research efforts that have made this thesis possible. I also gratefully acknowledge the reviewers of this thesis, Professor Kari Enqvist and Docent Aleksi Vuorinen, for their assessment of the thesis and constructive criticism. I am pleased that Professor Eduardo Fraga has agreed to be my opponent in the defence of my thesis and for that I would also like to thank him.

Another set of thanks belongs to the particle physics and cosmology community in the department. I would like to thank you all for interesting conversations about physics and mathematics, whether or not they have had any relation to this thesis. I have learned a great deal from these discussions. From the different people involved in this field I should mention Professor emeritus Vesa Ruuskanen, Professor Jukka Maalampi, Professor Kari J. Eskola and Docent Kimmo Kainulainen and thank them for their very interesting lectures. Particularly, I would like to thank Professor Kari J. Eskola for his support and express my admiration on the effort he puts in teaching. It has been (and will be) a pleasure to work with you all.

Furthermore, the rest of the research and administrative staff of the department have my gratitude as well for making this a great place to work. I have enjoyed the dinner table and coffee break conversations with my colleagues about science but also about a great variety of other subjects. A special acknowledgement goes to the Department of Physics football team, Atomin Pamaus, and it's players with whom I have played in several tournaments with no notable success.

Finally I would like to thank my parents and especially my wife Inkeri for all the support they have given me during the time I have worked on this thesis.

Jyväskylä, November 2010

Topi Kähärä

People

Author Topi Kähärä
Department of Physics
University of Jyväskylä
Finland

Supervisor Docent Kimmo Tuominen
Department of Physics
University of Jyväskylä
Finland

Reviewers Professor Kari Enqvist
Department of Physical Sciences
University of Helsinki
Finland

Docent Aleksi Vuorinen
Faculty of Physics
University of Bielefeld
Germany

Opponent Professor Eduardo Souza Fraga
Instituto de Física
Universidade Federal do Rio de Janeiro
Brasil

List of Publications

I Topi Kähärä and Kimmo Tuominen. *Degrees of freedom and the phase transitions of two–flavor QCD. Phys. Rev.*, D78:034015, 2008.

II Topi Kähärä and Kimmo Tuominen. *Effective models of two–flavor QCD: from small towards large m_q. Phys. Rev.*, D80:114022, 2009.

III Topi Kähärä and Kimmo Tuominen. *Effective models of two–flavor QCD: finite μ and m_q –dependence. Accepted for publication in Phys. Rev.*, D, 2010.

The author has done the theoretical and numerical calculations presented in papers [I–III] as well as participated in their writing process.

Contents

1 Introduction

1.1 The history of the strong interaction

The history of the strong interaction began early in the 20th century with the discovery of the atomic nucleus and its constituents the proton and the neutron. It was these discoveries that hinted towards the existence of a new type of interaction: to keep the nucleus together there had to exist a force powerful enough to overcome the repulsive electric forces exerted on the tightly packed protons in core of the atom. At this point the proton and neutron were considered elementary particles and attempts to explain the force that bounded the nucleons together were not satisfactory. The nature of the strong force remained a mystery for decades although the applications of nuclear physics were not hindered by this ignorance.

New light was shed into the mystery of the strong interaction by the discovery of the pion in 1947 and by the early 60's particle accelerators and cosmic ray experiments had found several new particles similar to the nucleons, collectively called hadrons. These new particles could be classified according to certain symmetries. As in the case of the periodic system of elements, this hierarchy suggested a more elementary structure and a new theoretical idea emerged to explain the number and properties of these newly found particles. The new idea was the quark model, introduced in 1964 [1]. It abandonned the elementary particle status of the hadrons and instead described all the hadrons as bound states of three different new fermionic particles called quarks, and their antiparticles, interacting through an unknown force. The quark model had great success in describing and predicting the properties of hadrons, but no experiment succeeded in observing quarks and their existence as real particles was doubted. It became also clear that the suggested quark composition of the hadrons required the quarks to have an additional quantum number, which became known as color. These and other problems in the simple quark model were resolved by the discovery of non-Abelian gauge theories and the further construction of *Quantum ChromoDynamics* (QCD) in the early 70's. In QCD the quarks have, in addition to their electric charge, a color charge that was mediated by the gluons. This new type of interaction was the previously elusive and mysterious strong force.

Today QCD is a firmly tested part of the standard model of particle physics, however, this does not mean that all about the strong interaction is known. Due to its non-abelian nature and confining properties, QCD is a hard theory to investigate, both

theoretically and experimentally. The work carried out in this thesis is an attempt to investigate one of the most interesting unresolved question regarding the strong interaction: the behaviour of strongly interacting matter at a very high density or temperature. In this context "very high" means several times denser than nuclear matter or thousands of times hotter than the core of the sun. The study of these extreme conditions might seem like a purely theoretical exercise, but it is not. Such conditions may be found inside exotic stellar bodies such as neutron stars and almost certainly existed right after the birth of our universe. Surprisingly, such conditions, can also be created and studied in the laboratory in relativistic heavy ion collisions.

1.2 Quark gluon plasma and heavy ion collisions

In the early 80's lattice QCD theorists proposed [2] that there exists a deconfined phase of quarks and gluons at a high temperature region of the theory. This phase is nowadays referred to as the *Quark Gluon Plasma* (QGP). One can imagine this phase as a system where the quarks and gluons have such high energies, that the asymptotic freedom of QCD allows them to travel freely in this medium. However, as one might expect, the experimental verification of such matter was still far away as experiments capable of producing it had to be designed and built.

The first hadron colliders ISR *(Intersecting Storage Rings)* and SPS *(Super Proton Synchrotron)* at CERN *(Organisation Européenne pour la Recherche Nucléaire)* as well as the later Tevatron at Fermilab collided mainly protons with fixed targets or with anti–protons and, although they made other great particle physics discoveries, they were not ideally suited for QGP production. It took until the year 2000 that RHIC *(Relativistic Heavy Ion Collider)*, a dedicated heavy ion collider, started taking data at BNL *(Brookhaven National Laboratory)* and now after a decade of running RHIC has provided compelling evidence that indeed QGP exists and can be produced in laboratory conditions. Alongside the continuing RHIC experiments the LHC *(Large Hadron Collider)* heavy ion program is about to start, attempting to produce hotter and larger volumes of QGP with longer lifetimes. Further down the line is the CBM *(Condensed Baryonic Matter)* experiment at the FAIR *(Facility for Antiprotons and Ions Research)* facility in Germany which is supposed to probe the high net baryon density region of the QCD phase diagram.

1.3 Outline of this thesis

Although experiments are compatible with the existence of QGP there is still much to learn about its properties and the phase structure of QCD in general. The work done

in this thesis aims to investigate some of the aspects still unknown about the phases of QCD. These include the location of the phase boundaries between hadronic matter and QGP, the order of the phase transitions and the existence of critical points in the (T, μ) –phase diagram. Also some thermodynamic variables such as the pressure, trace anomaly and quark number density are investigated.

The above mentioned QCD phenomena are studied in this thesis through the use of effective models that try to incorporate the key properties of QCD into a simpler and more easily solved framework. The hope is that these models could be then utilized to predict and explain observed strong interaction phenomena with reasonable accuracy.

The layout of this thesis is the following: In Chapter 2 the aspects of QCD that are incorporated into the models used in this thesis are introduced and also some lattice QCD results are discussed. In Chapter 3 the effective models studied in this thesis, as well the parameters used to set them up, are discussed in detail. Chapter 4 then presents the results published in papers [I, II, III] along with some yet unpublished results. Finally, this thesis is concluded in Chapter 5 where the future prospects of the effective model approach used in this thesis are discussed.

1.4 Notation

The notation in this thesis follows that of [3] and is commonly used in modern particle physics and field theory texts.

For relativistic quantummechanics we use the metric

$$g_{\mu\nu} = g^{\mu\nu} = \begin{pmatrix} 1 & 0 & 0 & 0 \\ 0 & -1 & 0 & 0 \\ 0 & 0 & -1 & 0 \\ 0 & 0 & 0 & -1 \end{pmatrix} \tag{1.1}$$

with the Greek indeces running over 0, 1, 2 and 3. The index 0 corresponds to the time coordinate, while indeces 1, 2 and 3 correspond to spatial directions. When Roman indeces i, j and k are used they run over 1, 2 and 3 and correspond to the three spatial directions. All repeated indeces are summed. The often used Dirac gamma matrices γ^0, γ^1 γ^2 and γ^3 are defined by their anticommutation relation

$$\{\gamma^\mu, \gamma^\nu\} = 2g^{\mu\nu}. \tag{1.2}$$

The fifth gamma matrix is defined as

$$\gamma^5 = i\gamma^0\gamma^1\gamma^2\gamma^3. \tag{1.3}$$

Also the three Pauli matrices are of importance:

$$\tau^1 = \begin{pmatrix} 0 & 1 \\ 1 & 0 \end{pmatrix}, \quad \tau^2 = \begin{pmatrix} 0 & -i \\ i & 0 \end{pmatrix}, \quad \tau^3 = \begin{pmatrix} 1 & 0 \\ 0 & -1 \end{pmatrix}. \tag{1.4}$$

The Pauli matrices obey the commutation relation

$$[\tau^i, \tau^j] = 2i\epsilon_{ijk}\tau^k, \tag{1.5}$$

where ϵ is the Levi–Civita antisymmetric symbol.

We use units in which $\hbar = c = 1$. This means that

$$[\text{mass}] = [\text{energy}] = [\text{time}]^{-1} = [\text{lenght}]^{-1}. \tag{1.6}$$

Most quantities are given in electronvolts (eV) but also in some cases femtometers (fm) are used. The relation between these is

$$1 \text{ MeV} = 5.0677 \cdot 10^{-3} \text{ fm}^{-1}. \tag{1.7}$$

2 Features of QCD

2.1 Introduction

In this chapter I will discuss some aspects of QCD relevant to the work presented in this thesis. First, in Section 2.2, I introduce the symmetry properties of QCD that are used as quidelines in building the effective models in Chapter 3. Second, in Section 2.3, I present results from lattice QCD calculations that motivate the use of effective models of the type studied in this thesis and also discuss results used to fit some of the parameters in these models. I will not go into these subjects in detail, rather I will give a very brief overview, since the emphasis of this thesis is in Chapters 3 and 4. In writing this chapter I have used the information presented in articles and textbooks [3–16] where the reader may find a much more detailed description of the properties of QCD discussed here. For those aspects of QCD, or gauge theories in general, that are not discussed here at all, I refer the reader to textbooks like e.g. [3].

2.2 Symmetries of QCD

2.2.1 The $SU(3)$ gauge symmetry

Quantum Chromodynamics is a non–Abelian gauge theory describing the interactions of elementary particles called quarks and gluons. These interactions are ultimately described by the QCD Lagrangian which is required to remain invariant under local $SU(3)$ gauge transformations with quark colors being the quantum numbers associated with this gauge group. In QCD the quarks are set to be in the fundamental, and the gluons in the adjoint, representation of the gauge group and thus the Lagrangian is

$$\mathcal{L}_{QCD} = \bar{\psi}_f(i\gamma^\mu D_\mu - m_f)\psi_f - \frac{1}{4}F_{\mu\nu}{}^a F^{\mu\nu a}. \tag{2.1}$$

Here ψ_f denote the quarks fields and γ^μ are the standard Dirac gamma matrices. The field strenght tensor $F_{\mu\nu}{}^a$ and the covariant derivative D_μ are defined as

$$D_\mu \equiv \partial_\mu - ig_s t^a A^a_\mu \tag{2.2}$$

$$F_{\mu\nu}{}^a \equiv \partial_\mu A_\nu{}^a - \partial_\nu A_\mu{}^a - g_s f^{abc} A_\mu{}^b A_\nu{}^c, \tag{2.3}$$

where A^a_μ are the gluon fields. The matrices t^a are the $SU(3)$ generators and f^{abc} is the group structure constant defined by the $SU(3)$ Lie algebra

$$[t^a, t^b] = if^{abc}t^c. \tag{2.4}$$

The Lagrangian (2.1) satisfies the requirement of local gauge invariance under the $SU(3)$ gauge transformations $U(x)$

$$\psi \to U(x)\psi \quad , \quad D_\mu \to U(x)D_\mu U^\dagger(x), \tag{2.5}$$

where the spacetime dependence of the gauge transformations can be arbitrary.

2.2.2 Flavour and chiral symmetries

In addition to the defining $SU(3)$ gauge symmetry QCD has other symmetry properties many of which are exact only with certain constraints. Two of these symmetries are the flavor symmetry and the chiral symmetry, both of which are related to the mass of the quarks.

Since in QCD quark flavors differ from each other only by their masses, setting the masses of two or more flavors equal will result in a $SU(N_f)$ symmetry that rotates the mass degenerate flavors. In reality the masses of the flavors differ and this accounts for the observed hadron masses, or rather their mass differences. However, since the two lightest quarks u and d have comparable masses that are small relative to the QCD scale, the $SU(2)$ flavor symmetry is a good approximate symmetry of QCD. This symmetry, if exact, would imply $m_u = m_d$ and is called the isospin symmetry. If exactly isospin symmetric, the Lagrangian (2.1) is invariant under the transformations

$$\psi \to U_{SU(2)}\psi, \tag{2.6}$$

where ψ is now a quark doublet consisting of u and d quarks. In the work that makes up this thesis we have assumed that the isospin symmetry is exact and the four heaviest quarks are considered too heavy to be excited and are thus ignored.

At the limit, where one takes the two lightest quark masses to zero (and ignores rest of the quarks), the QCD Lagrangian (2.1) has isospin symmetry, as described above, allowing transformations mixing the u and d quarks. However, due to the masslessness of the quarks, and thus a lack of coupling between left– and right–handed states, the Lagrangian now becomes symmetric under individual unitary rotations of left– and right–handed quarks as well

$$\psi_L \to U_{SU(2)_L}\psi_L, \quad \psi_R \to U_{SU(2)_R}\psi_R, \tag{2.7}$$

where the chiral components of the quark doublet are

$$\psi_L = \left(\frac{1-\gamma^5}{2}\right)\psi, \quad \psi_R = \left(\frac{1+\gamma^5}{2}\right)\psi. \tag{2.8}$$

This $SU(2)_L \times SU(2)_R$ is called the chiral symmetry. Chiral symmetry can be reformulated as a vector and an axial vector symmetry of the form $SU(2)_V \times SU(2)_A$, where the $SU(2)_V$ vector symmetry corresponds to the transformations $U_{SU(2)_L} = U_{SU(2)_R}$ i.e. the isospin symmetry and the axial vector symmetry $SU(2)_A$ then is made up from the transformations $U_{SU(2)_L} = U^{\dagger}_{SU(2)_R}$. The corresponding currents are the isospin and chiral currents,

$$J^i_\mu = \bar{\psi}\gamma_\mu\tau^i\psi \quad \text{and} \quad J^i_{5\mu} = \bar{\psi}\gamma_\mu\gamma_5\tau^i\psi, \tag{2.9}$$

respectively. Although neither chiral or isospin symmetry is exact in QCD, in view of experimental results the isospin current is approximately conserved, while the chiral current is not connected to any observed conservation law. This can be explained by the mechanism of spontaneous symmetry breaking that occurs in the QCD vacuum.

First consider the case where the quarks are massless. Then the energy cost of producing a quark anti–quark pair from the vacuum is very low. Since momentum and angular momentum are conserved, the produced quark and anti–quark will have opposite momentum and opposite spin, which results in net chirality of the pair. In a vacuum that contains a condensate of such pairs the expectation value $\langle\Omega|\bar{\psi}\psi|\Omega\rangle$ will obtain a non–zero value and since

$$\bar{\psi}\psi = \bar{\psi}_L\psi_R + \bar{\psi}_R\psi_L \tag{2.10}$$

this expectation value is not invariant under the axial transformations $SU(2)_A$. This means that the axial symmetry is not a symmetry of the vacuum, eventhough it is a symmetry of the Lagrangian. This phenomenon, in which the vacuum does not obey a symmetry of the Lagrangian, is called spontaneous symmetry breaking. The physical consequence of this is that, although the quarks have zero mass in the Lagrangian, they propagate through the vacuum as if they had significant masses.

Since $\langle\Omega|\bar{\psi}\psi|\Omega\rangle$ is invariant under the vector transformations $SU(2)_V$ the isospin symmetry is still respected by the vacuum and the isospin current is thus conserved. The spontaneous symmetry breaking pattern is then

$$SU(2)_V \times SU(2)_A \to SU(2)_V, \tag{2.11}$$

which corresponds to three broken continuous symmetries, one for each broken axial current. The Goldstone theorem tells us that we should find three massless spin zero particles that are generated by the spontaneous symmetry breaking.

If we now consider real QCD with explicitly broken axial symmetry i.e. the u and d quarks have small non–zero masses in the Lagrangian, the vacuum has net axial

charge in a similar fashion to the massless case since creating a pair of light quarks is not costly in terms of energy. Again a spontaneous symmetry breaking pattern occurs through the vacuum expectation value $\langle\Omega|\bar{\psi}\psi|\Omega\rangle$. However, now the axial charge is carried not only by the vacuum but also by the massive quarks. This means that the new particles created by this symmetry breaking are not massless and thus not true Goldstone bosons. In QCD the pions form an isotriplet of light mesons that can be considered as the isotriplet associated with the symmetry breaking.

In addition to the $SU(2)_V$ and $SU(2)_A$ symmetries the massless QCD Lagrangian has two singlet symmetries $U(1)_V$ and $U(1)_A$ which I have not discussed above. With these, the fermionic symmetry group of the Lagrangian can be written as

$$SU(2)_V \times SU(2)_A \times U(1)_V \times U(1)_A. \tag{2.12}$$

The axial $U(1)$ symmetry is however anomalously broken when the theory is quantized since it is not respected by the full quantum path integral. However, the vector $U(1)$ symmetry is respected by QCD and the corresponding conserved quantum number is the baryon number

$$j_\mu = \bar{\psi}\gamma_\mu\psi. \tag{2.13}$$

I will not discuss these $U(1)$ symmetries further here since they do not play a significant role in the work presented in this thesis.

2.2.3 The $Z(3)$ symmetry and deconfinement

Since QCD is, by construction, symmetric under local gauge transformations of the $SU(3)$ gauge group, it is also symmetric under subgroups of $SU(3)$. One of these is the center group of $SU(3)$

$$Z(3) = \{z \in SU(3) \,|\, zU = Uz \;\forall\, U \in SU(3)\} \tag{2.14}$$

i.e. the elements of $SU(3)$ that commute with all other elements of $SU(3)$. The $Z(3)$ group has three elements

$$\mathbf{1}, \quad \mathbf{1}e^{2\pi i/3} \quad \text{and} \quad \mathbf{1}e^{4\pi i/3} \tag{2.15}$$

each consisting of a unit matrix and a constant phase. Since the $Z(3)$ group has only a finite number of elements the group transformation cannot change continuously from point to point and thus it constitutes a global symmetry of the Lagrangian. Unlike the isospin and chiral symmetries, which are only approximate symmetries of the QCD Lagrangian, global $Z(3)$ symmetry is an exact symmetry of the Lagrangian.

Consider now QCD at finite temperature. In the imaginary time formalism the imaginary time coordinate τ is periodic with a period β corresponding to the inverse of

the temperature T and the boundary conditions for boson and fermion fields are then given by the quantum statistics for the corresponding fields, see e.g. [17]. The result is that bosons are required to be periodic with respect to τ while fermions must be anti–periodic. For QCD quarks and gluons this means:

$$\psi(0,\vec{x}) = -\psi(\beta,\vec{x}) \quad \text{and} \quad A_\mu(0,\vec{x}) = A_\mu(\beta,\vec{x}). \tag{2.16}$$

Since the Lagrangian is invariant under local $SU(3)$ transformations, let us see what happens to the boundary conditions:

$$\begin{aligned} \psi(0,\vec{x}) &\to U(0,\vec{x})\psi(0,\vec{x}) \\ \psi(\beta,\vec{x}) &\to U(\beta,\vec{x})\psi(\beta,\vec{x}) \end{aligned} \tag{2.17}$$

$$\begin{aligned} A_\mu(0,\vec{x}) &\to U^\dagger(0,\vec{x})A_\mu(0,\vec{x})U(0,\vec{x}) \\ A_\mu(\beta,\vec{x}) &\to U^\dagger(\beta,\vec{x})A_\mu(\beta,\vec{x})U(\beta,\vec{x}). \end{aligned} \tag{2.18}$$

Due to the quarks being in the fundamental representation their transformation involves only one transformation matrix and thus only periodic gauge transformations

$$U(0,\vec{x}) = U(\beta,\vec{x}) \tag{2.19}$$

do not violate the boundary conditions (2.16) for quarks. So, although the QCD Lagrangian is invariant under local $SU(3)$ transformations with arbitrary dependence on x, the finite temperature boundary conditions for the quarks require the transformations to be periodic in the imaginary time τ. The gluons, however, are adjoint fields and their transformations involve also the inverse of the transformation matrix which means that any transformation matrix that commutes with the gluon field A_μ will keep it unchanged. By definition, the $SU(3)$ matrices that commute with all possible gluon fields constitute the $Z(3)$ symmetry group. As a result transitions for the gluons need to be periodic only up to an element of $Z(3)$ i.e.

$$U(0,\vec{x}) = zU(\beta,\vec{x}) \quad \text{where} \quad z \in Z(3) \tag{2.20}$$

in order to satisfy the boundary conditions (2.16).

If we now consider a pure gauge QCD with no dynamical quarks, which is in essence the opposite of considering massless quarks, the finite temperature formulation is invariant with respect to the choice of z in (2.20). It is important to note that this $Z(3)$ symmetry arising from the boundary conditions is not the same as the $Z(3)$ symmetry of the Lagrangian, although it is related to it. The global symmetry $Z(3)$ of the Lagrangian requires that the fields are rotated by the same $Z(3)$ element at every point, particularly at $\tau = 0$ and $\tau = \beta$, and such rotations would be trivially periodic. Instead the $Z(3)$ symmetry of the boundary conditions is a symmetry under $Z(3)$ rotations of the gluon fields only at $\tau = \beta$.

As we saw with the $SU(2)_A$ axial symmetry, even though the field equations respect a symmetry, it does not mean that the vacuum of the theory does. To examine this in the case of the $Z(3)$ symmetry we need a quantity, an order parameter, that behaves similarly as the expectation value $\langle\Omega|\bar{\psi}\psi|\Omega\rangle$ in the case with axial symmetry breaking. For the center symmetry such a quantity is the Polyakov loop [6]

$$\ell(\vec{x}) = \frac{\mathrm{Tr}L(\vec{x})}{3}, \tag{2.21}$$

where $L(\vec{x})$ is the thermal Wilson line

$$L(\vec{x}) = \mathcal{P}\exp[\int_0^\beta ig_s A_0(\tau,\vec{x})d\tau]. \tag{2.22}$$

The $\mathcal{P}$ in (2.22) denotes path ordering i.e. the gauge fields in the power–series expansion of the exponential are in the order they appear in the taken path, with the beginning of the path being to the right.

Since in gauge transformations the Wilson line transforms as

$$L(\vec{x}) \to U^\dagger(\beta)L(\vec{x})U(0) \tag{2.23}$$

the Polyakov loop, as a trace of L, is invariant under periodic gauge transformation. However transformations of the type (2.20) lead to a transformation law

$$\ell(\vec{x}) \to z\ell(\vec{x}) \tag{2.24}$$

for the Polyakov loop. Now the vacuum expectation value $\langle\ell(\vec{x})\rangle$ of the Polyakov loop has to be zero in order for the vacuum to be invariant under the $Z(3)$ symmetry. This connection with the Polyakov loop also relates the $Z(3)$ symmetry to confinement.

The free energy for a static quark F_q can be written in term of the Polyakov loop [11,12]

$$F_q = -T\ln[\langle\ell(\vec{x})\rangle] \tag{2.25}$$

and the free energy of a static quark anti–quark pair can then be written as the correlation function of two Polyakov loops

$$F_{\bar{q}q}(\vec{x}-\vec{y}) = -T\ln[\langle\ell(\vec{y})^\dagger\ell(\vec{x})\rangle]. \tag{2.26}$$

A vanishing vacuum expectation value for the Polyakov loop then implies an infinite free energy for a single quark or, in the case of the quark anti–quark correlator, an infinite pair potential. These imply quark confinement and thus the Polyakov loop can also be considered as an order parameter for confinement. In [16] the interpretation of the Polyakov loop as the free energy of a static quark is challenged since the expectation value $\langle\ell(\vec{x})\rangle$ can be complex while the free energy must be always real.

Instead it is suggested that the Polyakov loop should be understood as the propagator of the quark and confinement is then equivalent with a vanishing propagator.

Since in real QCD with finite temperature and finite mass quarks the $Z(3)$ symmetry is broken explicitly also the Polyakov loop will be always non–zero at finite temperature. This means that at finite temperature total confinement does not occur. However, at low temperatures we still expect $\ell(\vec{x}) \approx 0$. And since the QCD coupling g_s runs and approaches zero at high energies, one could then expect the absolute value of the Polyakov loop to approach one at high temperatures signalling a strongly deconfined phase. Between these extremes one would naturally expect to find a phase transition. This is similar to the chiral symmetry case where the broken symmetry of the vacuum becomes less broken at high tempreratures, conversely in the $Z(3)$ symmetry case the symmetry is broken at high temperature and is a better symmetry at lower energies. The order of the deconfinement transition may depend on several factors, particularly the masses of the lightest quarks including the s quark, see [18]. In QCD, lattice simulations indicate that the deconfinement transition is a crossover, see [19] or Figure 2.2.

2.3 On lattice QCD

One approach to solving QCD is evaluating the necessary functional integrals on a discrete spacetime lattice. This method was first envisioned by Wilson in [20]. The lattice approach is unique in its ability to study non-perturbative aspects of QCD by simulating the complete QCD Lagrangian, thus making it a very powerful albeit expensive tool. Here, however, I will not discuss lattice formulation of QCD nor numerical methods, for those I refer the reader to reviews such as [13]. Instead, I will discuss some results and aspects of lattice QCD that motivate the use of effective models such as the ones studied in this thesis.

Since the first Monte Carlo simulations [9], one of the goals of lattice QCD has been the study of the QCD equation of state. This involves the study of phase transition such as the chiral and deconfinement transitions. Early lattice studies showed that these seemingly unrelated transitions occur at the same temperature in QCD [13, 21, 22]. This is illustrated in Figure 2.1 where the chiral and deconfinement order parameters are shown along with their susceptibilities. The coincidence of these two transitions then might suggest that they are, in fact, related somehow. The conclusion would then be that in order to describe correctly the QCD phase diagram with respect to either one of these transition one has to take into account the other as well. This is also then reflected in the models that attempt to describe these phenomena. The models used in this thesis, PNJL and PLSM, are good examples of models that take lattice findings, like the one discussed, as a guideline in choosing the relevant degrees

of freedom present in the models. More recent lattice studies [19, 23] have found out that the coincidence of the two transitions is not perfect, see Figure 2.2. Still the relative closeness of the two transitions necessitates the inclusion of them both into models describing QCD phase transition phenomena.

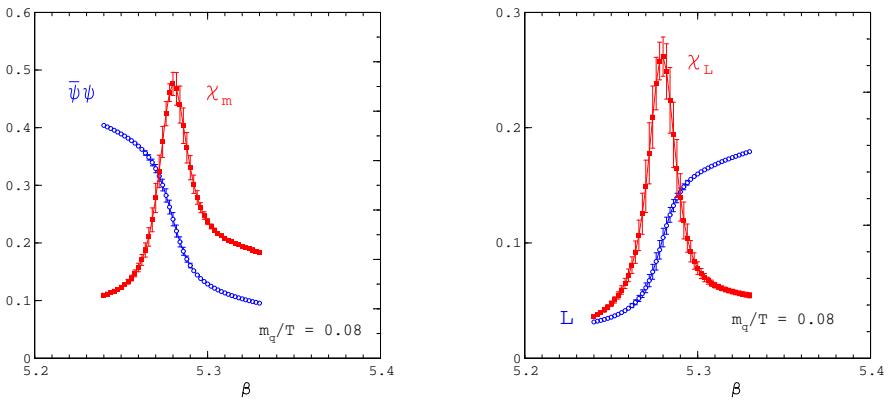

Figure 2.1: The behaviour of the chiral condensate, the Polyakov loop and their susceptibilities as seen in lattice simulations. Figures from [18].

One might wonder why use effective models in the first place if the exact QCD Lagrangian can be studied by lattice methods. The answer is simple: QCD is a very hard theory to solve and although lattice calculations are a precise way of studying QCD, they require a lot of computing power and definite answers to several questions cannot be answered by the power of todays computers. Also the study of non–zero baryon number density on the lattice has great inherent problems, in addition to the need of considerable computer time. At non–zero baryon number density the fermion matrix becomes complex and this makes the direct application of Monte Carlo simulation techniques impossible [13], although the functional integrals themselves are well defined even in this case. Different methods such as reweighing, Taylor expansion and analytic continuation, have been suggested to overcome this problem [24], but still the study of the QCD phase diagram away from the $\mu = 0$ line on the lattice is very exploratory [25].

In the work constituting this thesis we have used effective models that do not have the constraints of the lattice when it comes to computer power or doing calculations at finite baryon density. However, lattice results such as [26–29] are nevertheless needed to fit several parameters in the models. Thus, lattice calculations and effective models should be viewed as complementary approaches in describing strongly interacting phenomena. In the next chapter I will describe in detail the models studied in this thesis as well as the fits to lattice data that go into these models.

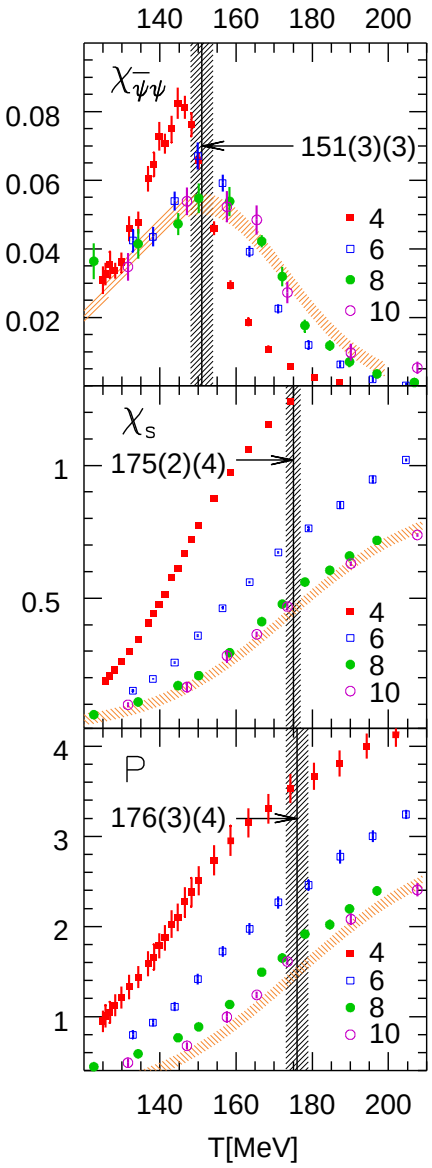

Figure 2.2: The temperature dependence of the chiral susceptibility $\chi_{\bar{\psi}\psi}$, the strange quark number susceptibility χ_s and the renormalized Polyakov loop P as seen on the lattice [19]. The solid vertical lines indicate the critical temperatures for each transition.

3 The effective model approach

3.1 Overview

Although perturbative attempts to describe the QCD phase diagram exist [30], there are great difficulties with this approach, particularly at low energies where perturbation theory breaks down, and thus several effective theories are used instead of QCD to describe the phenomena associated with the strong interaction. All of these effective theories retain some essential features of QCD, but have a reduced degree of complexity. Of course the features one should choose depend on the phenomena one is interested in.

As discussed in Chapter 2, the QCD phase diagram can be drawn with the transition lines of chiral symmetry and deconfinement. In this work we have studied models that incorporate the two approximate symmetries of QCD that govern these transitions: the chiral symmetry and the $Z(3)$ symmetry. The chiral symmetry is described by two different models that have been used since the 60's: the Nambu-Jona-Lasinio (NJL) model and the linear sigma model (LSM). The $Z(3)$ symmetry is then added to these models through a static background field that couples to quarks and a lattice data fitted potential describing the symmetry breaking. The resulting combinations are then called the Polyakov extended Nambu-Jona-Lasinio model or linear sigma model abbreviated PNJL and PLSM, respectively. In recent years the interest in these type of models has been abundant and they have been studied for example in [31–57].

In the following sections I will write down the Lagrangians for the models used in this thesis and verify that their symmetry properties indeed correspond to those of QCD.

3.2 The model Lagrangians

3.2.1 The NJL model

The Nambu-Jona-Lasinio (NJL) model was originally constructed as a theory of nucleons before the appearance of QCD [58]. The modern variants of the theory exhibit quark degrees of freedom instead of the nucleons. I will not discuss the history of the

model or its variants. Instead, I will present the model used in the work presented in this thesis. For a review on the NJL model, see e.g. [59].

We consider the NJL model with only the two lightest quark flavors: u and d. The model Lagrangian is

$$\mathcal{L} = \bar{q}(i\gamma^\mu\partial_\mu - m_q)q + \frac{G}{2}\left[(\bar{q}q)^2 + (\bar{q}i\gamma_5\vec{\tau}q)^2\right], \tag{3.1}$$

where $\vec{\tau}$ are the Pauli matrices. If the quark masses are zero i.e the matrix m_q is zero, then indeed the Lagrangian is chirally symmetric. This can be seen by applying the $SU(2)_A$ transformation to the quark fields

$$q \to \exp[-i\frac{\tau\cdot\theta}{2}\gamma_5]q. \tag{3.2}$$

By using

$$\exp[\pm i\vec{\theta}\cdot\vec{\tau}] = \cos|\theta| \pm i\frac{\vec{\theta}\cdot\vec{\tau}}{|\theta|}\sin|\theta| \tag{3.3}$$

we get

$$\begin{aligned}(\bar{q}q) &\to (\bar{q}q)\cos\theta - (\bar{q}i\gamma_5\hat{\theta}\cdot\vec{\tau}q)\sin\theta \\ (\bar{q}i\gamma_5\tau_i q) &\to (\bar{q}i\gamma_5\tau_i q) + (\bar{q}q)\hat{\theta}_i\sin\theta - (\bar{q}i\gamma_5\vec{\theta}\cdot\vec{\tau}q)\hat{\theta}_i(1-\cos\theta),\end{aligned} \tag{3.4}$$

where $\hat{\theta}_i = \theta_i/|\theta|$. Inserting (3.4) into the Lagrangian (3.1), we see that the sum of $(\bar{q}q)^2$ and $(\bar{q}i\gamma_5\vec{\tau}q)^2$ is invariant in the transformation. The kinetic term $\bar{q}(i\gamma^\mu\partial_\mu)q$ is in itself invariant under (3.3) since the matrix γ_5 commutes with any pair of γ matrices. However, since $(\bar{q}q)$ was not alone invariant neither can the mass term $(m_q\bar{q}q)$ be, and so the Lagrangian (3.1) is invariant under (3.3) only if $m_q = 0$.

Since chiral symmetry is explicitly broken in QCD we will also break it explicitly in our effective models. This means that we will keep the mass term m_q and assign a small mass for the quarks. We will, however, retain isospin symmetry i.e. invariance under the $SU(2)_V$ transformations

$$q \to \exp[-i\frac{\tau\cdot\omega}{2}]q. \tag{3.5}$$

This symmetry is preserved if we have degenerate masses for the two quark flavors.

3.2.2 The linear sigma model

The linear sigma model has a history comparable to the NJL model, but again I will only discuss the particular model used in the work presented in this thesis.

The linear sigma model we use features the sigma meson and the pions, their mutual interactions and interactions with quarks. The Lagrangian is

$$\mathcal{L} = \bar{q}\left(i\gamma^\mu\partial_\mu - g(\sigma + i\gamma_5\vec{\tau}\cdot\vec{\pi})\right)q + \frac{1}{2}(\partial_\mu\sigma\partial^\mu\sigma + \partial_\mu\vec{\pi}\cdot\partial^\mu\vec{\pi}) + U(\sigma,\vec{\pi}), \tag{3.6}$$

where the potential is

$$U(\sigma,\vec{\pi}) = \frac{m^2}{2}(\sigma^2+\pi^2) + \frac{\lambda^2}{4}(\sigma^2+\pi^2)^2 - H\sigma. \tag{3.7}$$

We will use the form

$$U(\sigma,\vec{\pi}) = \frac{\lambda^2}{4}(\sigma^2+\pi^2-v^2)^2 - H\sigma, \tag{3.8}$$

which is equivalent to (3.7) with $v^2 = -m^2/\lambda^2$.

Now the term $-H\sigma$ acts as the symmetry breaking term similarly to the quark mass in the NJL model. If we set $H = 0$ and apply the $SU(2)_A$ transformations

$$\begin{aligned} q &\to \exp[-i\frac{\tau\cdot\theta}{2}\gamma_5]q \simeq (1 - i\frac{\tau\cdot\theta}{2}\gamma_5)q \\ \sigma &\to \sigma' \simeq \sigma - \pi\cdot\theta \\ \vec{\pi} &\to \vec{\pi}' \simeq \vec{\pi} + \sigma\vec{\theta} \end{aligned} \tag{3.9}$$

the Lagrangian stays invariant. This also holds for the $SU(2)_V$ transformations

$$\begin{aligned} q &\to \exp[-i\frac{\tau\cdot\omega}{2}]q \simeq (1 - i\frac{\tau\cdot\omega}{2})q \\ \sigma &\to \sigma' = \sigma \\ \vec{\pi} &\to \vec{\pi}' \simeq \vec{\pi} - \pi\times\omega. \end{aligned} \tag{3.10}$$

Again we want to retain the isospin symmetry and break the chiral symmetry explicitly making it only approximate as in QCD. This is achieved by the inclusion of the term $-H\sigma$ in (3.8). One can easily verify that it conserves the $SU(2)_V$ symmetry but breaks the $SU(2)_A$ symmetry.

3.2.3 The Polyakov extension

The NJL and LSM Lagrangians presented in the previous sections have the desired chiral and isospin symmetry properties and now we need to add the $Z(3)$ symmetry to the models. This is done by adding a lattice fitted mean field potential for the Polyakov loop to the Lagrangians (3.1) and (3.6). To connect the chiral and pure

gauge sectors the coupling between a static background gauge field and the quarks is also introduced.

We start with the definition of the thermal Wilson line L

$$L = \mathcal{P} \exp[\int_0^\beta i g_s A_0(\vec{x}, \tau) d\tau], \tag{3.11}$$

where g_s is the gauge coupling and A_0 is defined as $A_0 = A_0^a \frac{\lambda_a}{2}$. Here A_0^a are the $SU(3)$ gauge fields and λ_a are then the Gell-Mann matrices. In the work presented here we consider only the A_0 component of the field and treat it as a constant static background field i.e. independent of $\vec{x}$ and τ. The Polyakov loop is defined as the color trace of the thermal Wilson line

$$\ell = \frac{\mathrm{Tr}_c L}{N_c} \tag{3.12}$$

and is included in our Lagrangians through a mean field potential

$$U_\ell \equiv U(\ell, \ell^*, T) = \left(-\frac{b_2(T)}{2} |\ell|^2 - \frac{b_3}{6}(\ell^3 + \ell^{*3}) + \frac{b_4}{4}(|\ell|^2)^2 \right) T^4, \tag{3.13}$$

where the coefficient b_2 depends on the temperature

$$b_2(T) = a_0 + a_1 \left(\frac{T_0}{T}\right) + a_2 \left(\frac{T_0}{T}\right)^2 + a_3 \left(\frac{T_0}{T}\right)^3. \tag{3.14}$$

The parameters a_0, a_1, a_2, a_3, b_3 and b_4 are fitted to the lattice data from pure gauge theory. The values of these parameters will be discussed in Section 3.4.3. While the potential (3.13) used in our work is a simple polynomial obtained from [35], logarithmic forms for the potential also exist [33,37,45]. These forms have advantages over the simple polynomial form such as contraining the Polyakov loop ℓ to be always smaller than 1 [37]. However, in [45] it was found that the polynomial form (3.13) is consistent with the logarithmic potentials used in [37, 45] at temperatures up to 300 MeV. Since this temperature is approximately $1.5\,T_c$ we can safely use the polynomial potential to investigate the phase transition. It is also worth to mention that both the polynomial and logarithmic versions of the potential contain only traces of the Wilson loop, although the center symmetry would allow also terms such as $\mathrm{Tr}[L^3 + L^{\dagger 3}]$.

In [III] we also consider a μ–dependent Polyakov potential, where the dependence on the chemical potential was introduced through the critical temperature T_0. We use the parametrisation

$$T_0(\mu) = T_\tau e^{-1/(\alpha_0 b(\mu))} \tag{3.15}$$

introduced in [42] and used also for example in [44]. This parametrisation is based on perturbative estimates on how the QCD running coupling α is changed by fermionic contributions. The μ–dependence is in the coefficient $b(\mu)$, which also depends on the number of quark flavors and colors. I will discuss the form we use for $b(\mu)$ and also the values of the parameters α_0 and T_τ in Section 3.4.3.

3.3 Model thermodynamics

3.3.1 The mean field approximation

We study the model thermodynamics in the mean field approximation. This is done in a slightly different way in the PLSM and PNJL models due to the different degrees of freedom in the models. However, the approximation scheme used will result in quite similar mean field potentials for the two models.

Mean field approximation in the PNJL model

The mean field approximation in the PNJL model involves the linearization of the quadratic quarks fields. This is achieved by the following expansion around the vacuum expectation values

$$(\bar{q}q) \to \langle\bar{q}q\rangle + (\bar{q}q)_f, \quad (\bar{q}i\gamma_5\vec{\tau}q) \to \langle\bar{q}i\gamma_5\vec{\tau}q\rangle + (\bar{q}i\gamma_5\vec{\tau}q)_f, \tag{3.16}$$

where the subscript f now denotes a small fluctuation. Inserting this expansion to the Lagrangian (3.1) and neglecting the squares of the fluctuations, one gets

$$\begin{aligned}\mathcal{L}_{\mathrm{PNJL}} = \bar{q}\left(i\gamma^\mu(\partial_\mu - g_s A_0\delta_{\mu 0}) - m_q + G(\langle\bar{q}q\rangle + i\gamma_5\vec{\tau}\cdot\langle\bar{q}i\gamma_5\vec{\tau}q\rangle)\right)q \\ + \frac{G}{2}\left(\langle\bar{q}q\rangle^2 + \langle\bar{q}i\gamma_5\vec{\tau}q\rangle^2\right) + U_\ell.\end{aligned} \tag{3.17}$$

Similarly as in the PLSM case we can simplify also the PNJL model further by setting $\langle\bar{q}i\gamma_5\vec{\tau}q\rangle = 0$. Again this can be done due to the fact that in an isospin symmetric system the pseudoscalar isotriplet has a zero expectation value.

As in the PLSM case we write the PNJL mean field Lagrangian in terms of the constituent quark mass which is $M = m_q - G\langle\bar{q}q\rangle$ in the PNJL case. The Lagrangian then is

$$\mathcal{L}_{\mathrm{PNJL}} = \bar{q}\left(i\gamma^\mu(\partial_\mu - g_s A_0\delta_{\mu 0}) - M\right)q + U_\chi + U_\ell, \tag{3.18}$$

where the chiral potential is

$$U_\chi = \frac{(m_q - M)^2}{2G}. \tag{3.19}$$

Mean field approximation in the PLSM model

In the mean field approximation for the PLSM case we replace the meson fields with their vacuum expectation values and neglect possible mesonic fluctuations. This implies

$$\sigma \to \langle\sigma\rangle \quad \vec{\pi} \to \langle\vec{\pi}\rangle \tag{3.20}$$

and

$$\partial_\mu \langle \sigma \rangle \to 0 \quad \partial_\mu \langle \vec{\pi} \rangle \to 0. \tag{3.21}$$

After these approximations have been made the PLSM mean field Lagrangian is

$$\begin{aligned} \mathcal{L}_{\text{PLSM}} = \bar{q} \left(i\gamma^\mu (\partial_\mu - g_s A_0 \delta_{\mu 0}) - g(\langle \sigma \rangle + i\gamma_5 \vec{\tau} \cdot \langle \vec{\pi} \rangle) \right) q \\ + \frac{\lambda^2}{4} \left(\langle \sigma \rangle^2 + \langle \pi \rangle^2 - v^2 \right)^2 - H \langle \sigma \rangle + U_\ell, \end{aligned} \tag{3.22}$$

A further simplification arises from the unbroken isospin symmetry. In an isospin symmetric system the expectation value of a pseudoscalar isotriplet is zero, for us this implies $\langle \vec{\pi} \rangle = 0$. Here we see the importance in the way we broke chiral symmetry in the model. The symmetry breaking term in the potential (3.8) was $-H\sigma$, this term, linear in the sigma field, does not alter the fact that $\langle \vec{\pi} \rangle = 0$. If we had broken the symmetry with a term that would also break the isospin symmetry this property would have been lost.

We now write the Lagrangian in its final form

$$\mathcal{L}_{\text{PLSM}} = \bar{q} \left(i\gamma^\mu (\partial_\mu - g_s A_0 \delta_{\mu 0}) - M \right) q + U_\chi + U_\ell, \tag{3.23}$$

where we have introduced the constituent quark mass $M \equiv g \langle \sigma \rangle$ and the chiral potential is

$$U_\chi = \frac{\lambda^2}{4} \left(\left(\frac{M}{g} \right)^2 - v^2 \right)^2 - \frac{HM}{g}. \tag{3.24}$$

3.3.2 Derivation of the grand potential

In this section I will show how to obtain the grand potential from the model Lagrangians (3.18) and (3.23). This derivation follows the one presented in [17].

The model Lagrangians (3.18) and (3.23) differ slightly but can be both expressed in the form

$$\mathcal{L} = \bar{q}(i\gamma^\mu(\partial_\mu - g_s A_0 \delta_{\mu 0}) - M)q + U, \tag{3.25}$$

where the q– and $\bar{q}$–independent potential U now includes the chiral potentials of the models (3.19) or (3.24) and the Polyakov potential (3.13). Also it is important to remember that the quark fields q and $\bar{q}$ have, in addition to their Dirac indeces, indeces of color and flavor, although they are omitted for the most part in order to keep the notation tidy.

The first thing to do is to calculate the partition funtion $\mathcal{Z}$ since all thermodynamics can be derived from it. It is given as a functional integral

$$\mathcal{Z} = \int \mathcal{D}\bar{q}(\mathbf{x}, \tau) \int \mathcal{D}q(\mathbf{x}, \tau) \exp \left[\int_0^\beta d\tau \int_V d^3x \left(\mathcal{L} + \mu \bar{q} \gamma^0 q \right) \right], \tag{3.26}$$

which is written in imaginary time formalism, where $\tau = it$ and $\beta = 1/T$ with T being the temperature. Inserting the Lagrangian into (3.26) we immediately get

$$\mathcal{Z} = \exp\left[\frac{UV}{T}\right] \int \mathcal{D}\bar{q}(\mathbf{x},\tau) \int \mathcal{D}q(\mathbf{x},\tau) \exp\left[\int_0^\beta d\tau \int_V d^3x\, \bar{q}\, D\, q\right], \tag{3.27}$$

where D now denotes the matrix

$$D \equiv \left(i\gamma^\mu \partial_\mu - M + (-ig_s A_0 + \mu)\gamma^0\right). \tag{3.28}$$

Note that the potential U comes directly out accompanied with the integration volumes since it is not only independent of the quark fields but also of $\mathbf{x}$ and τ. In order to do the functional integrals in (3.27) we discretize the action

$$S \equiv \int_0^\beta d\tau \int_V d^3x\, \bar{q}\, D\, q \tag{3.29}$$

by switching from $(\mathbf{x},\tau)$-space to $(\mathbf{p},\omega_n)$-space. This is done by discretizing the quark fields using the following Fourier transformation

$$q(\mathbf{x},\tau) \;=\; \frac{1}{\sqrt{V}} \sum_{n=-\infty}^{\infty} \sum_{\mathbf{p}=-\infty}^{\infty} \exp\left[i(\mathbf{p}\cdot\mathbf{x} + \omega_n \tau)\right] \hat{q}(\mathbf{p},n) \tag{3.30}$$

where the discrete frequency must be $\omega_n = (2n+1)\pi T$ in order to keep the fermion fields antiperiodic. By inserting (3.30) into the action (3.29), operating with the matrix D and cancelling out the exponential factors, one gets

$$S = \int_0^\beta d\tau \int_V d^3x\, \frac{1}{V} \sum_n \sum_{\mathbf{p}} \hat{\bar{q}}(\mathbf{p},n)\, \hat{D}\, \hat{q}(\mathbf{p},n), \tag{3.31}$$

where

$$\hat{D} = -\gamma^\mu p_\mu - M + (-ig_s A_0 + \mu)\gamma^0 \tag{3.32}$$

and $p_\mu = (i\omega_n, \mathbf{p})$. The integrals over $\mathbf{x}$ and τ are now trivial and can be performed to obtain the result

$$S = \frac{1}{T} \sum_n \sum_{\mathbf{p}} \hat{\bar{q}}(\mathbf{p},n)\, \hat{D}\, \hat{q}(\mathbf{p},n). \tag{3.33}$$

Now we can insert this discretized action into the partition function (3.27), rewrite the functional integrals as a product and obtain

$$\mathcal{Z} = \exp\left[\frac{UV}{T}\right] \prod_{n,\mathbf{p},d,f,c} \int d\hat{\bar{q}}_{d,f,c}(\mathbf{p},n) d\hat{q}_{d,f,c}(\mathbf{p},n) \exp\left[S\right], \tag{3.34}$$

where the product is over momentum $\mathbf{p}$, frequency ω_n, Dirac indeces d, color c and flavor f. Recalling the integral formula

$$\int d\psi_1^\dagger d\psi_1 \cdots d\psi_N^\dagger d\psi_N \exp\left[\psi^\dagger\, D\, \psi\right] = \det D \tag{3.35}$$

for Grassmann variables $\psi_1 \cdots \psi_N$ and $\psi_1^\dagger \cdots \psi_N^\dagger$, we can now do the integrals in (3.34) and arrive at a deceivingly simple formula

$$\mathcal{Z} = \exp\left[\frac{UV}{T}\right] \frac{\det_{\mathbf{p},n,d,f,c} \hat{D}}{T}, \tag{3.36}$$

where the determinant is taken again over momentum $\mathbf{p}$, frequency ω_n, Dirac indeces d, color c and flavor f. To make progress, we turn to the definition of the grand potential

$$\Omega = -\frac{T}{V} \ln \mathcal{Z} \tag{3.37}$$

and by inserting (3.36), the potential separates into two terms

$$\Omega = -U - \Omega_{\bar{q}q} \tag{3.38}$$

where U is still the quark–independent part of our initial Lagrangian (3.25) and the term with the quarks integrated out is simply

$$\Omega_{\bar{q}q} \equiv \frac{T}{V} \ln\left[\frac{\det \hat{D}}{T}\right]. \tag{3.39}$$

Here we can utilize the connection

$$\ln \det \hat{D} = \mathrm{Tr} \ln \hat{D} \tag{3.40}$$

and write

$$\Omega_{\bar{q}q} = \frac{T}{V} \sum_n \sum_{\mathbf{p}} \mathrm{Tr}_{c,f} \ln\left[\frac{\det_d \hat{D}}{T}\right], \tag{3.41}$$

where the sums correspond to traces over n and $\mathbf{p}$ and the Dirac determinant is left to be taken over the matrix $\hat{D}$. The remaining determinant can be evaluated as follows

$$\begin{aligned} \det \hat{D} = &\quad \det\left(-\gamma^\mu p_\mu - M + (-ig_s A_0 + \mu)\gamma^0\right) \\ = &\quad \left(M^2 + |\mathbf{p}|^2 - (-ig_s A_0 + \mu - p_0)^2\right)^2 \\ = &\quad \left((\omega_n + i(-ig_s A_0 + \mu - p_0))^2 + E^2\right)^2, \end{aligned} \tag{3.42}$$

where $E^2 = M^2 + |\mathbf{p}|^2$. The potential is then

$$\Omega_{\bar{q}q} = \frac{T}{V} \sum_n \sum_{\mathbf{p}} \mathrm{Tr}_{c,f}\, 2 \ln\left[\beta^2 \left((\omega_n + i(-ig_s A_0 + \mu))^2 + E^2\right)\right]. \tag{3.43}$$

Since the frequencies ω_n are summed over both negative and positive values one can make subsititution $\omega_n \to -\omega_n$ without changing the sum. With this in mind we write

$$\begin{aligned} \Omega_{\bar{q}q} = \frac{T}{V} \sum_n \sum_{\mathbf{p}} \mathrm{Tr}_{c,f}\ &\ln\left[\beta^2 \left((\omega_n + i(-ig_s A_0 + \mu))^2 + E^2\right)\right] \\ &+ \ln\left[\beta^2 \left((-\omega_n + i(-ig_s A_0 + \mu))^2 + E^2\right)\right] \end{aligned} \tag{3.44}$$

and after some algebra we arrive in

$$\begin{aligned}\Omega_{\bar{q}q} = \frac{T}{V}\sum_n \sum_{\mathbf{p}} \mathrm{Tr}_{c,f}\ \ln\left[\beta^2\left(\omega_n^2 + (E-(\mu - ig_sA_0))^2\right)\right] \\ + \ln\left[\beta^2\left(\omega_n^2 + (E+(\mu - ig_sA_0))^2\right)\right].\end{aligned} \tag{3.45}$$

The frequency summation can be done using methods presented for example in [17]. The result is

$$\Omega_{\bar{q}q} = 2T\int \frac{d^3p}{(2\pi)^3}\mathrm{Tr}_{c,f}\left(\beta E + \ln\left[1+Le^{-\beta(E-\mu)}\right] + \ln\left[1+L^\dagger e^{-\beta(E+\mu)}\right]\right), \tag{3.46}$$

where $L = \exp[ig_sA_0\beta]$ and $L^\dagger = \exp[-ig_sA_0\beta]$ are now the Polyakov loop matrices.

Finally the remaining traces have to be calculated. The trace over flavor gives in our case a factor 2 since we are only dealing with two degenerate flavors. The trace over color is a little more complicated since the Polykov loop matrices have color structure. However in the so called Polyakov gauge [60] the Polyakov loop matrix can be written in a convenient diagonal form

$$L = \mathrm{diag}\left(e^{i\theta_1}, e^{i\theta_2}, e^{-i(\theta_1+\theta_2)}\right). \tag{3.47}$$

We use (3.40) again and evaluate the resulting determinant

$$\begin{aligned}&\mathrm{Tr}\ln\left[1+Le^{-\beta(E-\mu)}\right] \\ &= \ln\det\left[1+Le^{-\beta(E-\mu)}\right] \\ &= \ln\left[1+\mathrm{Tr}(L)e^{-\beta(E-\mu)} + \mathrm{Tr}(L^\dagger)e^{-2\beta(E-\mu)} + e^{-3\beta(E-\mu)}\right].\end{aligned} \tag{3.48}$$

With this result, we can now write the whole grand potential (3.38) as

$$\begin{aligned}\Omega = -U - 4\int \frac{d^3p}{(2\pi)^3}\, 3E \\ + \ln\left[1+3\left(\ell + \ell^* e^{-\beta(E-\mu)}\right)e^{-\beta(E-\mu)} + e^{-3\beta(E-\mu)}\right] \\ + \ln\left[1+3\left(\ell^* + \ell e^{-\beta(E+\mu)}\right)e^{-\beta(E+\mu)} + e^{-3\beta(E+\mu)}\right].\end{aligned} \tag{3.49}$$

This potential is then used to solve the thermodynamics of the two models with U including the appropriate chiral potential for the NJL and LSM cases. Also, the divergent term in (3.49) is treated differently in NJL and LSM: In the NJL case the divergent term is included and regulated by a cut–off while in the LSM case two different approaches are used. In [I, II] the vacuum term was omitted in LSM and in [III] a renormalized form was used. This will be discussed in more detail in Sections 3.4.1 and 3.4.2.

3.3.3 Solving the thermodynamics

Once we have derived the grand potential for our models we can proceed to evaluate the thermodynamics. This is achieved by first solving the equations of motion for the three order parameters

$$\frac{\partial\Omega}{\partial M}=0,\quad \frac{\partial\Omega}{\partial \ell}=0,\quad \frac{\partial\Omega}{\partial \ell^*}=0. \tag{3.50}$$

We use M as the order parameter for chiral symmetry rather than $\langle q\bar{q}\rangle$ or σ which are typically used in the NJL ans LSM models. We feel that using the same physical quantity for this purpose in both models aids in comparing the results. Here it should also be noted that ℓ and ℓ^* are treated as independent real variables in this minimization process, although they by definition are complex. This approximation is done to avoid the problems arising from minimizing a complex potential. In [38] the minimization is done to the real part of Ω and ℓ and ℓ^* are replaced with temporal gauge fields θ_1 and θ_2 that appear in the Polyakov gauge presentation for L [33]. It is then found that treating ℓ and ℓ^* as independent real quantities without taking into account the reality contraints for the gauge fields overestimates the difference between ℓ and ℓ^*. This overestimation is however not of great importance in our work since we are mainly interested in the qualitative behaviour of the models.

After solving the equations of motion (3.50) the pressure $p(T,\mu)$ is then simply

$$p(T,\mu)=\Omega(T,\mu) \tag{3.51}$$

with the potential evaluated at its minimum. Other thermodynamic quantities such as entropy density $s(T,\mu)$, energy density $\epsilon(T,\mu)$ and quark number density $n_q(T,\mu)$ can then be obtained from the pressure

$$s(T,\mu)=\frac{\partial p}{\partial T},\quad \epsilon(T,\mu)=Ts(T,\mu)-p(T,\mu),\quad n_q(T,\mu)=\frac{\partial p}{\partial \mu}. \tag{3.52}$$

The phase boundaries in the (T,μ)–plane can be studied through the order parameters M, ℓ and ℓ^*. The constituent quark mass M is the order parameter for the chiral symmetry and the Polyakov loops ℓ and ℓ^* describe the deconfinement transition. In Chapter 4 the methods used to determine the phase transition are discussed.

3.4 Model parameters

There are several parameters in both NJL and LSM chiral models as well as in the Polyakov potential that have to be set before any numerical work can be done. Most of the parameter sets we use are based on literature [31, 35] and used widely. In the

following sections I will go through the various parameters that have to be set, the values we have chosen for them. I will also discuss the extension of the models to unphysical pion masses.

3.4.1 Setting the NJL model parameters

In NJL model Lagrangian (3.1) we had two parameters: the quark mass m_q and the four-fermion coupling G. Also, since the coupling G has dimension $(\text{mass})^{-2}$, the model is non–renormalizable and to regulate the resulting divergent integrals, such as the vacuum energy term in (3.49), we introduce an additional parameter Λ, which acts as a momentum cut–off. The baseline for these parameters is set by choosing them so that they reproduce the vacuum values of the pion decay constant and the pion mass. In [II, III] we also studied the models away from the physical point i.e. the observed QCD vacuum by varying the amount of explicit chiral symmetry breaking.

Parameters at the physical point

At the physical point we want to set the parameters m_q, G and Λ so that the model is consistent with the measured values for the pion mass and the pion decay constant. Both quantities can be calculated also from the model. We use the mean field formulas calculated in [61] using the ring approximation. The pion mass is then the smallest non–zero solution to the equation

$$1 - G\frac{N_c N_f}{\pi^2}\,\mathbf{P}\int_0^\Lambda \frac{p^2}{E}\left(1 - \frac{m_\pi^2}{m_\pi^2 - 4E^2}\right)(1 - n_q - n_{\bar{q}})\,dp = 0 \tag{3.53}$$

and the pion decay constant can be obtained from the equation

$$f_\pi = \frac{G_{\pi q} M N_c N_f}{4\pi^2}\,\mathbf{P}\int_0^\Lambda \frac{p^2}{E(E^2 - \frac{1}{4}m_\pi^2)}\,(1 - n_q - n_{\bar{q}})\,dp, \tag{3.54}$$

where the pion quark coupling is

$$G_{\pi q}^2 = \frac{4\pi^2}{N_c N_f}\left[\mathbf{P}\int_0^\Lambda \frac{Ep^2}{(E^2 - \frac{1}{4}m_\pi^2)}\,(1 - n_q - n_{\bar{q}})\,dp\right]^{-1}. \tag{3.55}$$

In the above equations $\mathbf{P}$ denotes a principal value integral. The quark and anti-quark number densities are given by

$$n_q = \frac{1}{1 + \exp[(E - \mu)/T]} \quad n_{\bar{q}} = \frac{1}{1 + \exp[(E + \mu)/T]}. \tag{3.56}$$

The parameters m_q, G and Λ are set to values shown in Table 3.1. Using (3.53) and (3.54) we see that these values correspond to $m_\pi = 140$ MeV and $f_\pi = 94$ MeV. Also the sigma mass m_σ can be calculated from the model [61] and is given by the smallest non–zero solution to the equation

$$1 - G\frac{N_c N_f}{\pi^2}\,\mathbf{P}\int_0^\Lambda \frac{p^2}{E}\left(1 - \frac{m_\pi^2 - 4M^2}{m_\pi^2 - 4E^2}\right)(1 - n_q - n_{\bar{q}})\,dp = 0. \tag{3.57}$$

With our choice of parameters the sigma mass obtained from the model is $m_\sigma = 657$ MeV.

Table 3.1: Nambu–Jona–Lasinio model parameters corresponding to the QCD vacuum. The exact values are assigned by hand and the approximate values arise from the model.

m_q	Λ	G
5.5 MeV	651 MeV	10.08 $(\text{GeV})^{-2}$
f_π	m_π	m_σ
≈ 94 MeV	≈ 140 MeV	≈ 657 MeV

The model away from the physical point

In the NJL model the extension to larger explicit chiral symmetry breaking is in principle simple since the bare quark mass m_q, which is the origin of the broken chiral symmetry, is a direct parameter of the model. However, it is not clear if the other parameters of the model, G and Λ, should evolve when m_q is changed. In Figure 3.1 the pion mass obtained from the NJL model is compared to a lattice fit is used to parametrize the LSM model in Section 3.4.2. Although the two curves agree at low m_q the NJL overshoots the lattice result at higher m_q. Thus, in order to get an better agreement, we should tune the parameters G and Λ so that the NJL curve would come down. In Figure 3.2 the G– and Λ–dependence of the pion mass is shown for three different quark mass values with the dashed vertical line indicating our choice of parameters. Because the vertical line is close to the minima of the pion mass curves, the pion mass cannot be significantly lowered for a given m_q by tuning either G or Λ. This result leads us to conclude that the agreement of the NJL model with the lattice data cannot be improved tuning G or Λ. Thus the values for G and Λ determined at the physical point need not be changed when considering the model away from the physical point.

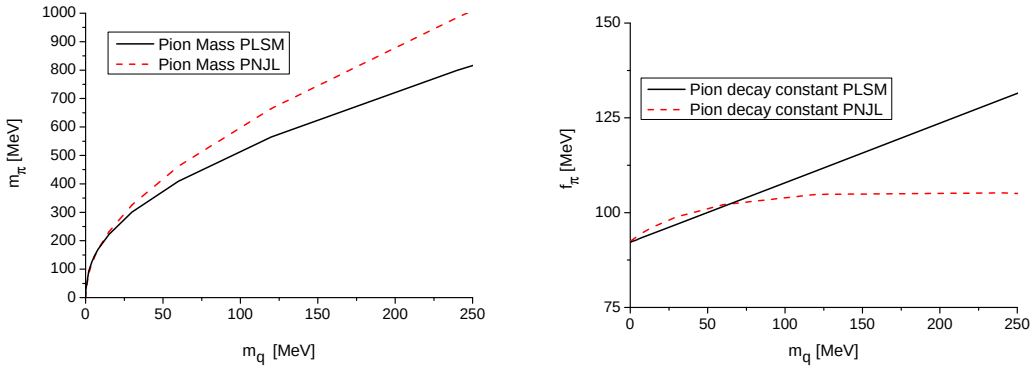

Figure 3.1: Pion mass m_π and pion decay constants f_π as functions of the bare quark mass m_q in the PLSM and PNJL models. The PLSM curves are based on a lattice parametrization discussed in Section 3.4.2 while the PNJL curves can be obtained using Equations (3.53) and (3.54).

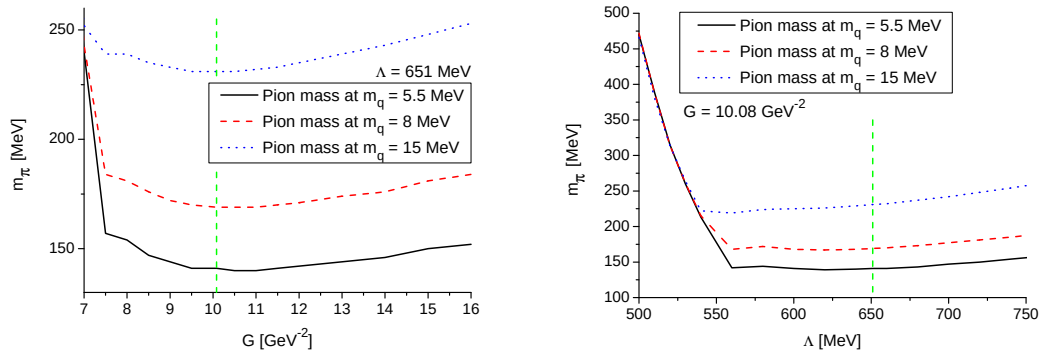

Figure 3.2: The dependence of the pion mass on the parameters G and Λ in the PNJL model. The pion mass is obtained from Equation (3.53).

3.4.2 Setting the LSM parameters

Parameters at the physical point

The LSM Lagrangian (3.6) has four adjustable parameters g, λ, v and H. As with the NJL case we want to set the parameters so that the model is consistent with observed values for the pion decay constant, pion mass and sigma mass. When one neglects the vacuum energy contribution that appears in (3.49), as we have done in [I, II], these quantities can be determined in the model by taking derivatives of the chiral potential

(3.8) with respect to the pion and the sigma fields. The zeros of the derivatives

$$\begin{aligned} \frac{\partial U}{\partial \sigma} &= \lambda^2(\sigma^2+\pi^2-v^2)\sigma - H = 0 \\ \frac{\partial U}{\partial \pi} &= \lambda^2(\sigma^2+\pi^2-v^2)\pi = 0 \end{aligned} \tag{3.58}$$

give the condition for the expectation values of the fields i.e. the minimum of the potential. The latter condition is satisfied by $\langle\pi\rangle = 0$ and the sigma expectation value is identified with the pion decay constant $\langle\sigma\rangle = f_\pi$. The pion and sigma masses are then obtained by evaluating the second derivatives of the potential

$$\begin{aligned} \frac{\partial^2 U}{\partial \sigma^2} &= \lambda^2(3\sigma^2+\pi^2-v^2) \\ \frac{\partial^2 U}{\partial \pi^2} &= \lambda^2(\sigma^2+3\pi^2-v^2) \end{aligned} \tag{3.59}$$

at the minimum resulting in

$$m_\sigma^2 = \lambda^2(3f_\pi^2 - v^2) \quad \text{and} \quad m_\pi^2 = \lambda^2(f_\pi^2 - v^2). \tag{3.60}$$

The parameters λ, v and H can now be solved from the above equations giving us

$$\lambda^2 = \frac{m_\sigma^2 - m_\pi^2}{2f_\pi}, \quad v^2 = f_\pi^2 - \frac{m_\pi^2}{\lambda^2} \quad \text{and} \quad H = f_\pi m_\pi^2. \tag{3.61}$$

The physical values for the pion mass and decay constant as well as the sigma mass can be now inserted. We use the values shown in Table 3.2. The fourth parameter in the LSM case, g, is evaluated through the relation $M = gf_\pi$, where the constituent mass M is approximately one third of the nucleon mass. The coupling g is then set to $g = 3.3$, which corresponds to a nucleon mass ~ 1 GeV.

In [III] we included in LSM also the vacuum term of the potential (3.49) in its renormalized form

$$\Omega_{\bar{q}q}^{reg} = -\frac{6g^4}{8\pi^2}\sigma^4 \ln\left(\frac{g\sigma}{\Lambda}\right) \tag{3.62}$$

which we obtained from [56]. Here Λ is a renormalization scale parameter and we choose it to be equal with the cut–off in the NJL case i.e. we take $\Lambda = 651$ MeV. Including the vacuum term also effects the derivatives of the potential and results in new equations for the pion and sigma masses

$$\begin{aligned} m_\pi^2 = &\quad \lambda^2(f_\pi^2 - v^2) - \frac{6g^4}{8\pi^2}f_\pi^2\left[4\ln\left(\frac{gf_\pi}{\Lambda}\right)+1\right] \\ m_\sigma^2 = &\quad \lambda^2(3f_\pi^2 - v^2) - \frac{6g^4}{8\pi^2}f_\pi^2\left[12\ln\left(\frac{gf_\pi}{\Lambda}\right)+7\right]. \end{aligned} \tag{3.63}$$

The parameter λ and v can then be written as

$$\begin{aligned} \lambda^2 &= \frac{m_\sigma^2 - m_\pi^2}{2f_\pi} - \frac{6g^4}{8\pi^2}\left[4\ln\left(\frac{gf_\pi}{\Lambda}\right) + 3\right] \\ v^2 &= f_\pi^2 - \frac{m_\pi^2}{\lambda^2} - \frac{1}{\lambda^2}\frac{6g^4}{8\pi^2}\left[4\ln\left(\frac{gf_\pi}{\Lambda}\right) + 1\right]. \end{aligned} \tag{3.64}$$

The equation for H or the way how we set g are not affected by the inclusion of the vacuum term. Also, we use as input the same values for f_π, m_π and m_σ as in the case without the vacuum term, so the values of the physical observables are not affected by the inclusion of the vacuum term. Actually, it turns out that the only parameter changed by the inclusion of the vacuum term is v since with our choice of renormalization scale, $\Lambda = 651$ MeV, the contribution from the vacuum term to λ in (3.64) is negligible. This, however, holds only for the physical pion mass.

Table 3.2: Linear sigma model parameters corresponding to the QCD vacuum. The exact values are assigned by hand and the approximate values arise from the model. All the parameters are the same with and without the vacuum term included, except for v for which v_{vac} and v_{novac} denote the values with and without the vacuum term, respectively.

f_π	m_π	m_σ	g
93 MeV	138 MeV	600 MeV	3.3
v_{vac}	v_{novac}	H	λ
$\approx 1.56 \cdot 10^4$ MeV^2	$\approx 7.68 \cdot 10^3$ MeV^2	$\approx 1.77 \cdot 10^6$ MeV^3	≈ 4.44

The model away from the physical point

In considering the linear sigma model away from the physical point a little more effort is needed than in the NJL model case. In the LSM the chiral symmetry breaking is characterized by the parameter H. As discussed in the previous section H is related to the pion decay constant and the pion mass, which are not independent and are also related to the sigma mass. In order to set the model parameters consistently for different amounts of explicit chiral symmetry breaking we introduce a scheme to relate the parameters to each other using results obtained from lattice calculations [27–29]. To get maximum comparability with the NJL model we choose the bare quark mass as the tunable parameter that controls the amount of symmetry breaking, as it is in the NJL model, and relate the pion mass to it. The rest of the parameters are then given in terms of the pion mass.

In [27] the pion mass is related to the quark mass through the relation

$$m_\pi^2 a^2 = (A_1 (m_q a)^{\frac{1}{1+\delta}} + B(m_q a)^2), \tag{3.65}$$

which is based on quenched chiral perturbation theory [62]. In [27] the parameters A_1, B and δ are then fitted to lattice data. We adopt the values from [27] and they are shown in Table 3.3. The leftover parameter a is the lattice spacing which in [27] is obtained from the equation

$$\sqrt{2}f_\pi a = 0.06672 + 0.221820 \times (m_q a) \tag{3.66}$$

by evaluating it at $m_q = 0$ MeV and $f_\pi = 93$ MeV [1]. This gives a lattice spacing of $a = 0.505306$ GeV^{-1}. We, however, would want $f_\pi = 93$ MeV $\Leftrightarrow m_q = 5$ MeV, which would lead to a different lattice spacing and subsequently alter the parameters used to fit (3.66). Since we do not want to alter the fit parameters, we shift the value of f_π by a constant $C = 1.18$. From (3.66) we then get

$$m_q a = \frac{\sqrt{2}(f_\pi + C)a - 0.06672}{0.221820}. \tag{3.67}$$

In combination with (3.65) this gives the pion mass m_π in relation with the pion decay constant f_π. The pion mass and the pion decay constant are plotted in Figure 3.1 as functions of the bare quark mass.

We connect the sigma mass m_σ to the pion mass m_π through the relation

$$m_\sigma = \xi m_\pi^2 + D, \tag{3.68}$$

where the slope $\xi = 1.83$ GeV^{-1} is obtained from [28]. The constant D is set so that the vacuum value of the pion mass $m_\pi = 138$ MeV corresponds to the vacuum sigma mass $m_\sigma = 600$ MeV. This condition leads to $D = 565.15$ MeV.

The last parameter g in the linear sigma model was defined so that $gf_\pi = M_N/3$, where M_N is the nucleon mass. At the physical point $m_\pi = 138$ MeV the nucleon mass is ~ 1 GeV, but altering the pion mass will also affect the nucleon mass. We estimate the nucleon mass with a chiral perturbation theory formula

$$M_N = M_0 + 4C_1 m_\pi^2 - \frac{3g_A^2}{32\pi f_\pi^2} m_\pi^3 \tag{3.69}$$

obtained from [29] and truncated to $\mathcal{O}(m_\pi^3)$. In [II] we used a fit truncated to $\mathcal{O}(m_\pi^2)$, but found that this overestimated the coupling g to such extent that it would have large effects on the phase diagram. Therefore in [III] we included the $\mathcal{O}(m_\pi^3)$ –term in (3.69) in order to get a better approximation. The parameters C_1 and g_A in (3.69) are taken directly from the lattice fit made in [29] with only a small adjustment to C_1, which stays within the errors of the fit. The parameter M_0 is then set so that (3.69) in conjunction with $gf_\pi = M_N/3$ is consistent with $g = 3.3$ in the vacuum. Values for the parameters discussed above are listed in Table 3.3.

[1] The actual value stated in [27] is $f_\pi = 132$ MeV, but due to a different definition of f_π this corresponds to the value $\sqrt{2}f_\pi$ in our work.

Table 3.3: The parameters used to relate m_q with f_π, m_π, m_σ and g in the linear sigma model.

a	A_1	δ	B	C
0.505306 $(\text{GeV})^{-1}$	0.82725	0.16413	1.88687	1.18 MeV
D	ξ	M_0	C_1	g_A
565.15 MeV	1.83 $(\text{GeV})^{-1}$	868 MeV	0.9 $(\text{GeV})^{-1}$	1.267

3.4.3 Parameters for the Polyakov potential

In Section 3.2.3 we introduced the polynomial Polyakov potential (3.13). The parameters a_i and b_i can be fitted to reproduce pure gauge lattice data. We use the fit made in [35] to lattice data from [26]. The parameter values used are shown in Table 3.4. The pure gauge critical temperature T_0 is set at 270 MeV. In [35] it was found that in the two–flavor case a lower critical temperature $T_0 \approx 190$ MeV would be required to fit lattice data in [63]. This is consistent with the perturbation theory estimates presented in [42]. We, however, used the pure gauge critical temperature $T_0 = 270$ MeV in our calculations [I, II, III] since fitting lattice calculations precisely was not a main concern for us.

In addition to the parameters a_i and b_i of the potential, we need to set the parameters that govern the μ–dependence of the Polyakov potential we use in [III]. As mentioned in Section 3.2.3 the μ–dependence of the critical temperature, T_0, is implemented through the relation (3.15), which we have obtained from [42]. We also adopt the values for T_τ and α_0 determined also in [42] and shown in Table 3.4. For the coefficient b in (3.15) we use the form

$$b(\mu) = \frac{11N_c}{6\pi} - \frac{16N_f}{\pi}\frac{\mu^2}{T_\tau^2}, \tag{3.70}$$

where we have dropped one of the terms proportional to N_f that appear in [42]. This will result in $T_0(\mu = 0) = 270$ MeV whereas with the additional term the critical temperature would be, for our two–flavor case, $T_0(\mu = 0) = 208$ MeV. We thus drop this term to make comparison with the μ–independent case easier, since in that case the constant critical temperature is $T_0 = 270$ MeV.

Table 3.4: Polyakov potential coefficients

a_0	a_1	a_2	a_3	b_3	b_4	α_0	T_τ
6.75	-1.95	2.625	-7.44	0.75	7.5	0.304	1.770 GeV

4 Results

In this chapter I will go through the main results obtained in papers [I, II, III] upon which this thesis is based. The main focus of our work in papers [I, II, III] is the phase diagram of the PNJL and PLSM models in the (T, μ)–plane. Knowing that these kind of effective models are sensitive to the parameters used, we were not particularly interested in the absolute locations of the transition boundaries or critical points, nor did we aim to make exact fits to lattice data. Instead we focused on the qualitative and quantitative differences between the NJL and LSM cases with and without the Polyakov extension and their sensitivity to the bare quark mass. Also the possibility of recently advocated quarkyonic matter is studied along with a way of implementing chemical potential dependence into the Polyakov potential.

4.1 Pressure and trace anomaly

In [I] we studied how the pressure and the trace of the energy momentum tensor are affected by the inclusion of the Polyakov loop degrees of freedom into the LSM and NJL chiral models. The results are shown in Figure 4.1 where also a QCD result is plotted for comparison. The QCD curves in Figure 4.1 correspond to a pQCD calculation [64, 65] which is then at low temperatures matched to a resonance gas result from [66].

From Figure 4.1 it is evident that the inclusion of the Polyakov loop is necessary to obtain the Stefan–Boltzmann limit of QCD pressure. This can be explained by the degrees of freedom that are taken into account: In the pure LSM and NJL cases the degrees of freedom are those of the quarks but the inclusion of the Polyakov loop introduces also gluonic degrees of freedom to the models. The ideal gas pressure is

$$p_{SB} = \frac{\pi^2 T^4}{45}\left(g_g + g_q\right) = \frac{\pi^2 T^4}{45}\left((N_c^2 - 1) + \frac{7 N_c N_f}{4}\right). \tag{4.1}$$

For $N_c = 3$ and $N_f = 2$ the ratio of quark and gluon contributions is $g_g/g_q = 16/21 \approx 0.76$ which means roughly an 80% increase in the pressure when the gluonic degrees of freedom are included. This is what is observed between the models with and without the Polyakov extension. The pressure of the Polyakov extended models above T_c is in quite good agreement with the QCD result. Below T_c, PLSM and PNJL underestimate

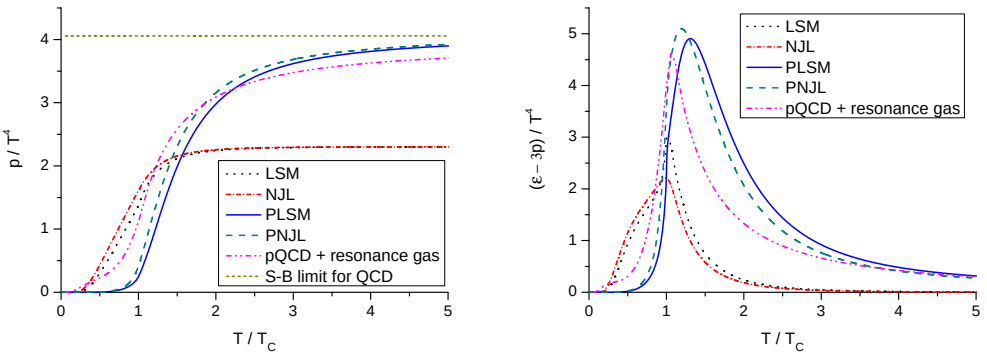

Figure 4.1: *Left panel*: Pressure from the models with and without the Polyakov loop at $\mu = 0$. Also shown is the curve interpolating between the resonance gas and resummed perturbation theory results [64] as well as the constant corresponding to the Stefan–Boltzmann limit of two-flavor QCD. *Right panel*: Similar figure for the trace anomaly $(\epsilon - 3P)/T^4$.

the pressure. This is, however, expected since the models do not contain the degrees of freedom relevant in the hadron gas region.

As with the pressure, the trace anomaly is better described by the Polyakov extended models than the purely chiral ones. In the LSM and NJL models there is a structure qualitatively different from the QCD result near T_c. The difference disappears in the PLSM and PNJL cases. Also the asymptotic behaviour of the trace anomaly is better described by the Polyakov extended models.

For a comparison between the model and QCD results for effective degrees of freedom

$$g_{\text{eff}} \equiv \frac{\epsilon(T)}{\left[\frac{\pi^2 T^4}{30}\right]}, \quad h_{\text{eff}} \equiv \frac{s(T)}{\left[\frac{2\pi^2 T^3}{45}\right]}, \quad i_{\text{eff}} \equiv \frac{c(T)}{\left[\frac{2\pi^2 T^3}{15}\right]}, \tag{4.2}$$

see [I]. Also results for the "equation of state parameter" $w(T) = p(T)/\epsilon(T)$ and the speed of sound $c_s(T) = \sqrt{\partial\epsilon/\partial p}$ can be found in [I] and will not be discussed here.

4.2 The phase diagram

4.2.1 The chiral transition and the critical point

The chiral transition can be accessed through the constituent quark mass M which can be treated as the order parameter for chiral symmetry in our models. Ideally an order parameter would have two discrete values, one in the symmetric phase and another in the phase of broken symmetry. However, as discussed in Chapter 3, we

have purposefully broken the chiral symmetry explicitly in the models we use since the symmetry is also explicitly broken in QCD. This leads to constituent quark mass behaviour such as shown in Figure 4.2, where M starts out large, but as temperature grows it drops rapidly at near a certain temperature and then asymptotically approaches zero. The value of M indicates the amount of chiral symmetry breaking, the smaller M is the closer the system is to chiral symmetry. If M would reach zero, then chiral symmetry would be again an exact symmetry.

Although there is no exactly chirally symmetric phase we still want to define a phase boundary between the chirally broken phase ($M \gg 0$) and the almost chirally symmetric phase ($M \approx 0$). In the case portrayed on the right hand side of Figure 4.2 the discontinuity in M is a natural choice for this phase boundary with a first order phase transition. This choice can be then extended to the continuous case shown on the left hand side of Figure 4.2 by defining the transition as the fastest point of change in order parameter. This point can be easily determined from the temperature derivatives of M, where it shows as a distinct peak. This is illustrated in Figure 4.3.

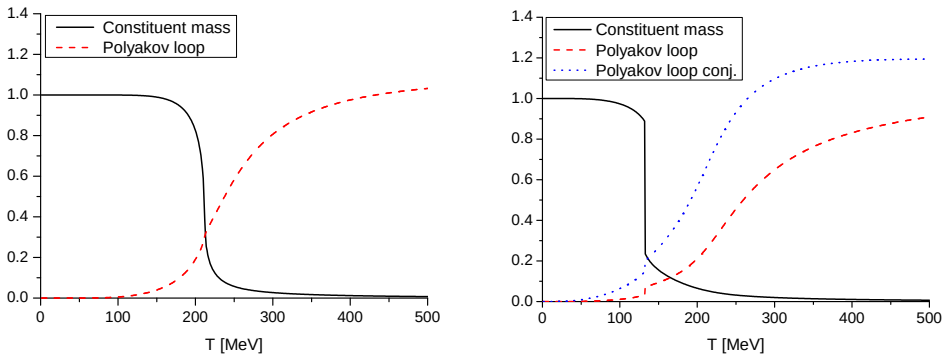

Figure 4.2: Constituent mass and Polyakov loop behaviour as a function of temperature in the PLSM model. Constituent mass normalized to unity at $T = 0$ MeV. *Left*: $\mu = 0$ MeV. *Right*: $\mu = 250$ MeV.

Effect of the Polyakov extension

In [I] we studied the differences between the two chiral models with (PNJL and PLSM) and without (NJL and LSM) the Polyakov extension. The resulting (T, μ)– phase diagrams are shown in Figures 4.4, where the solid lines represent a first order transition ending in the critical points denoted by the different symbols. The dotted part of the curves is the crossover transition determined from the peak in the temperature derivative.

One immediately sees that including the Polyakov degrees of freedom increases the

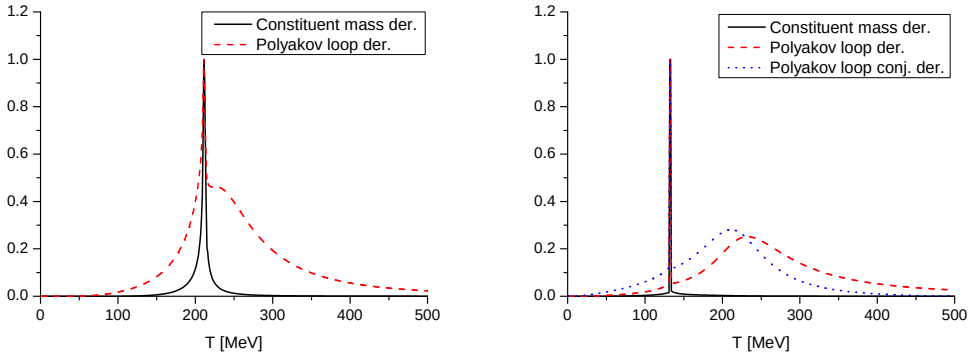

Figure 4.3: Constituent mass and Polyakov loop temperature derivative behaviour as a function of temperature in the PLSM model. Derivatives normalized to unity at maximum. *Left*: $\mu = 0$ MeV. *Right*: $\mu = 250$ MeV.

area of the chirally broken phase i.e. making the transition temperature higher for a given chemical potential. Also it brings the chiral transitions of the two models closer when at zero chemical potential [I].

The critical points, however, move even further apart with the Polyakov extension which could be due to several reasons. Maybe some important degrees of freedom, such as the diquarks [38], are being missed or as recently suggested in [56, 57] the vacuum terms in LSM should be regulated and included in the calculation. We did the inclusion of the vacuum terms for the LSM case in [III] and it is discussed in Section 4.2.1. In any case both models exhibit a similar behaviour and contain a critical point in the (T, μ)–plane. The critical point locations are summarized in Table 4.1.

Table 4.1: Critical temperatures at $\mu = 0$, critical chemical potentials at $T = 0$ and critical point locations for LSM, NJL, PLSM and PNJL models as observed in [I]. All values are in MeV.

LSM			**NJL**		
$T_c(\mu = 0)$	$\mu_c(T = 0)$	CP (T, μ)	$T_c(\mu = 0)$	$\mu_c(T = 0)$	CP (T, μ)
147	305	(99,207)	178	345	(33,334)
PLSM			**PNJL**		
$T_c(\mu = 0)$	$\mu_c(T = 0)$	CP (T, μ)	$T_c(\mu = 0)$	$\mu_c(T = 0)$	CP (T, μ)
212	345	(195,141)	230	345	(88,329)

Varying the bare quark mass

Effects of varying the bare quark mass m_q were studied in [I, II, III]. The bare quark mass is a direct input parameter of the PNJL model and the parameters of the linear

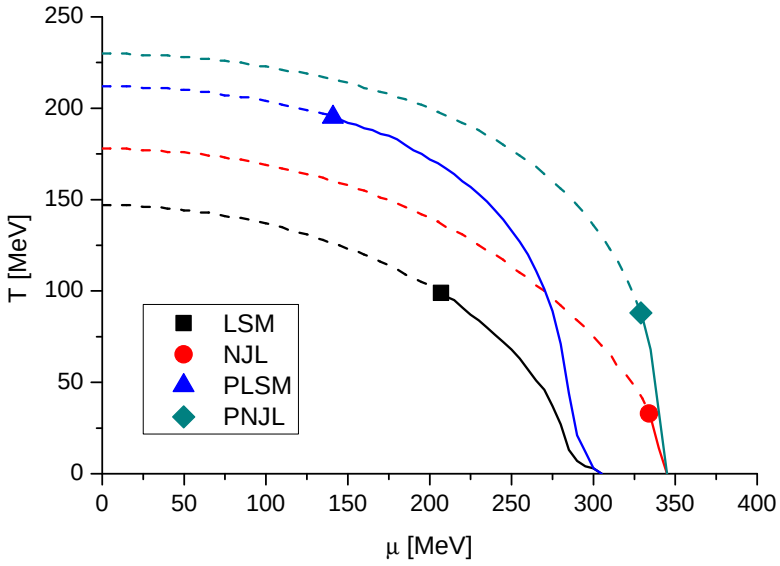

Figure 4.4: Comparison of the chiral transition boundaries and critical points in LSM, NJL, PLSM and PNJL. The dashed lines correspond to a crossover transition while the solid lines represent a first order transition. The critical points are portrayed by the different symbols. Figure from [I].

sigma model could also be given in terms of it as described in Chapter 3. It is also the parameter governing the amount of chiral symmetry breaking and thus varying it could give us valuable information on the dynamics between the chiral and Polyakov sectors. It turns out, however, that varying the bare quark mass has very little effect on the deconfinement transition described by the Polyakov order parameters ℓ and ℓ^*. This will be discussed in more detail in Section 4.2.2. One the other hand, the chiral transition, as one might expect, is affected greatly by the amount of explicit symmetry breaking.

The chiral phase diagrams for several quark masses are shown in Figures 4.5, 4.6 and 4.7 for PLSM with and without the quark vacuum contribution and PNJL, respectively. One immediately sees that the qualitative features between the models are quite similar: An increase in the bare quark mass from its physical value expands the area of the broken phase shifting the transition higher in T at $\mu = 0$ and higher in μ at $T = 0$. The opposite is true for a decrease in the quark mass. Also the quantitative differences in transition temperature are below 15 % between the models for the quark masses shown in Figure 4.5, indicating that the quark mass scaling works well. Despite the overall similarity in shape and location of the phase boundaries, the critical point seems to move quite differently in the different cases.

In PLSM, when the fermionic vacuum fluctuations are taken into account, the critical

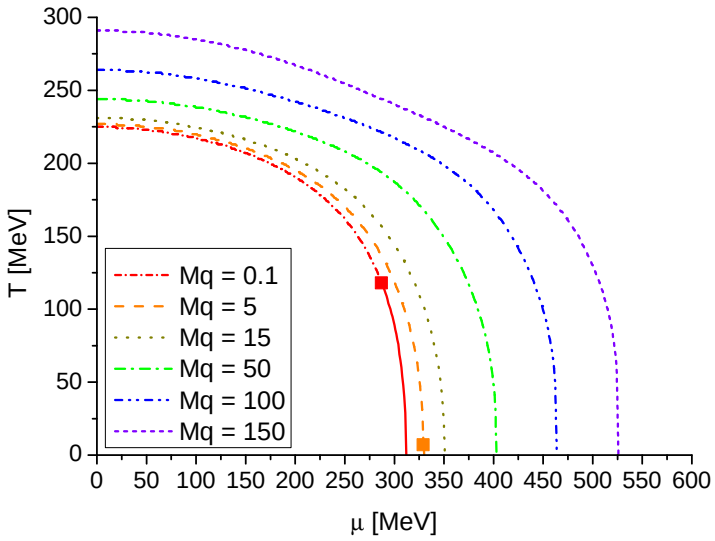

Figure 4.5: The chiral phase diagram of PLSM, with the fermion vacuum contribution included, for several quark masses. The solid curves indicate a first order (discontinuous) transition with the critical endpoints marked by squares. The locations of the critical points are summarized in Table 4.2.

point is present only for the two lowest quark masses studied and for higher quark masses the transition is a crossover throughout the plane. The result for the physical quark mass $m_q = 5$ MeV is compatible with results obtained in [57] and [67], although both references exhibit higher temperatures for the critical point. Also the value of m_q above which there is no critical point is similar to [50]. Without the fermionic vacuum fluctuations, the critical point seems to exist only at a finite m_q interval with the transition being completely first order at low m_q and a complete crossover at high m_q. A similar result has been obtained for a three flavor linear sigma model with a different method of controlling the amount of chiral symmetry breaking in [47]. The locations of the critical points with and without the vacuum term are given in Table 4.2.

In contrast to the PLSM case where the critical point was present only at a some values of m_q, the PNJL model critical point is observed for all studied quark masses. Since the fermion vacuum energy is included in the PNJL model, the critical point persists for the smallest quark masses as we would expect in light of the PLSM results. However, in the high m_q region the critical temperature at the critical point starts to rise when going towards larger quark masses having a low point between quark masses of 15 and 50 MeV. This is strikingly different behaviour than in the PLSM case. A similar result was observed in [38], where a saturation of the critical point temperature was mentioned and attributed to a diquark dominated phase. Our work

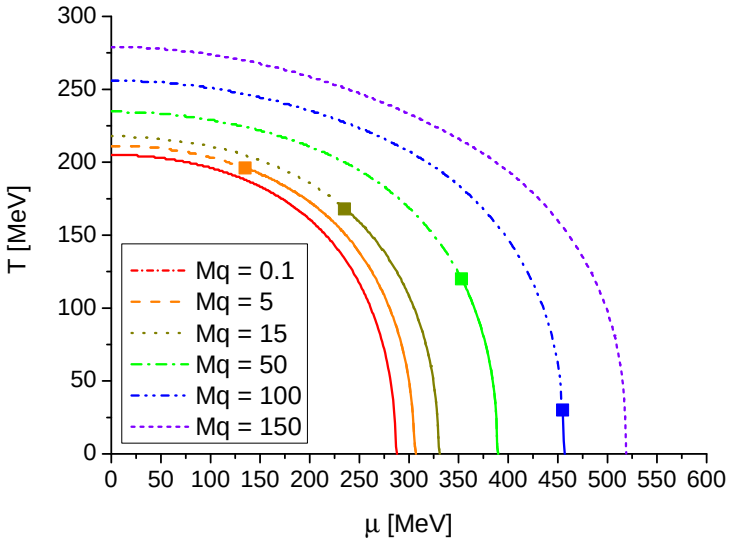

Figure 4.6: The chiral phase diagram of PLSM, without the fermion vacuum contribution, for several quark masses. The solid curves indicate a first order (discontinuous) transition with the critical endpoints marked by squares. The locations of the critical points are summarized in Table 4.2.

does not include diquarks, so we conclude that this behaviour is a more generic feature of the PNJL model. In [68] the Cornwall-Jackiw-Tomboulis effective potential in the improved-ladder approximation was used in a two–flavor QCD calculation where the minimum $T_c(\mu)$ appears at nearly the same values of m_q as in our analysis of the PNJL model. However, the temperatures of the critical points vary clearly more in [68] than in the PNJL model.

In either case multiple critical points as suggested for example in [69] or [50] were not observed.

4.2.2 The deconfinement transition

The deconfinement properties of our models arise from the Polyakov loop variables ℓ and ℓ^* introduced in Chapter 3. The deconfinement transition can be determined from these variables using different methods. As with the chiral transition, temperature (or chemical potential) derivatives can be used, as we did in [I, II], or one could use chiral susceptibilities. However, the use of derivatives gave rise to the double peak problem in which the chiral transition induces a double peaked structure in the derivative of the Polyakov order parameters making it difficult to consistently assign a critical temperature in all cases [I, II]. The double peak structure is illustrated in Figure 4.3.

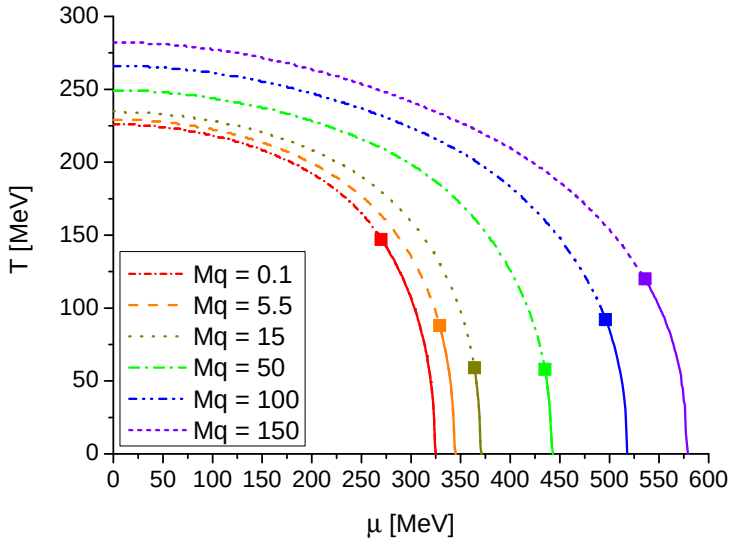

Figure 4.7: The chiral phase diagram of PNJL for several quark masses. The solid curves indicate a first order (discontinuous) transition with the critical endpoints marked by squares. The locations of the critical points are summarized in Table 4.2.

For deconfinement transitions determined from the softer peaks, see [I]. The double peak issue is not further discussed here. For details, see [I, II].

In [III] we adopted a method to determine the deconfinement from the absolute value of the Polyakov loop variables. Since in PLSM and PNJL deconfinement is achieved through numerical suppression of quark states with colour by ℓ and ℓ^*, it is a natural choice to associate the amount of confinement to the values of ℓ and ℓ^*. Ideally the values of the Polyakov loop variables would lie between 0 and 1, where 0 means total confinement and 1 means total deconfinement. However, due to our choice of potential, see Chapter 3, ℓ and ℓ^* range from 0 to ≈ 1.2 with the values over 1 actually giving an enhacement of colored states over colorless ones. Anyway, the deconfinement transition occurs between values from 0 to 1, so the values $\ell = 1/2$ and $\ell^* = 1/2$ are a good choice to be the indicator of when the system turns from a mostly confined state to a mostly deconfined state. Also in [III] the two transitions associated with ℓ and ℓ^* were replaced with their average in order to simplify the analysis and increase the readability of figures.

Deconfinement without explicit μ–dependence

A Polyakov potential without an explicit μ–dependence was considered in [I, II, III]. As discussed above, in [I, II] the deconfinement transition was determined from the

Table 4.2: Bare quark masses with corresponding pion masses and critical points for both models. In the PLSM case there are separate entries for the critical point for the cases where the vacuum term is either included or omitted. In the cases where there is no critical end point, the order of the transition is given. All values are in MeV.

PLSM				**PNJL**		
m_q	m_π	CP (T,μ) with vacuum term	CP (T,μ) w/o vacuum term	m_q	m_π	CP (T,μ)
0.1	26	(118,297)	Totally 1st order	0.1	19	(147, 270)
5	138	(8,325)	(196, 135)	5.5	140	(88, 329)
15	222	Totally crossover	(168, 235)	15	231	(59, 364)
50	377	Totally crossover	(120, 353)	50	421	(58, 435)
100	518	Totally crossover	(30, 455)	100	603	(92, 496)
150	629	Totally crossover	Totally crossover	150	752	(120, 536)

derivatives of ℓ and ℓ^* and in [III] the absolute values of ℓ and ℓ^* were used. In Figure 4.8 are the phase diagrams with the deconfinement now determined from the absolute value of the average of the Polyakov order parameters [III]. The differences between the two methods are small and the qualitative behaviour is identical. However, with the latter method we are able to consistently assign a transition temperature for deconfinement even when it is close to the chiral transition.

At the physical point $m_q \approx 5$ MeV, portrayed in Figures 4.8, the deconfinement transition lines for both PLSM and PNJL cases are located near $T \approx 230$ MeV at $\mu = 0$ MeV and slowly curve downwards as μ increases. Since the pure gauge potential, see Chapter 3, has a constant transition temperature of 270 MeV with no μ–dependence, the coupling to the chiral models brings the deconfinement transition temperature down closer to the chiral transition and induces a slight μ–dependence on it. However, the two models exhibit almost identical deconfinement transition lines despite difference in the chiral transitions, which indicates that the deconfinement transition is insensitive to the amount of chiral symmetry breaking. This is confirmed by increasing the bare quark mass to 50 MeV as shown in Figure 4.9. Although the T_c of the chiral transition increases by ~ 10 % at zero μ, the deconfinement transitions are almost unaffected. So, if one has tuned the Polyakov potential (or the chiral sector) in such a way as to obtain coincidence of the chiral and deconfinement transitions in a certain chiral model and for a certain quark mass, the coincidence will not hold for other quark masses or chiral models. In other words: the PLSM and PNJL type models do not exhibit a mechanism that would automatically force the chiral and deconfinement transitions to occur simultaneously at $\mu = 0$. Since recent lattice studies [19, 23] show that the two transitions do not happen at exactly the same temperature at $\mu = 0$, the lack of this feature in the PLSM and PNJL models is not alarming. Also the weak μ–dependence in the deconfinement transition makes it impossible to have coincidence of two transitions for μ beyond ~ 100 MeV due to the strong μ–dependence of the chiral transition. Whether or not in QCD the chiral

and deconfinement transitions stay close to each other also at finite μ remains to established, however, in the next section a method of achieving this in the effective model framework is presented.

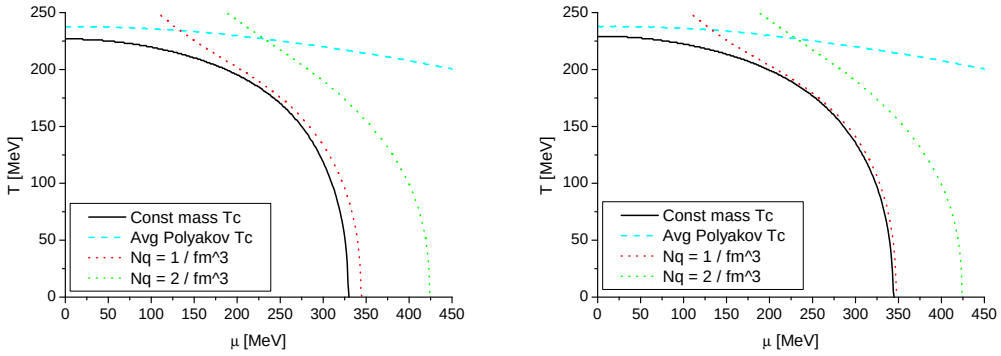

Figure 4.8: The phase diagrams of the models at the physical point $m_q \approx 5$ MeV with no explicit μ–dependence in the Polyakov potential. The solid line is the chiral transition and the dashed line the deconfinement transition. The dotted lines correspond to quark number densities of 1 fm^{-3} and 2 fm^{-3}. *Left*: PLSM with fermion vacuum contributions. *Right*: PNJL.

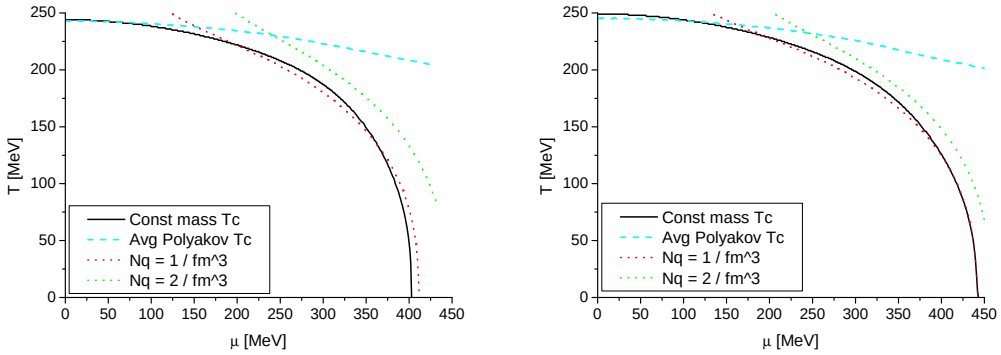

Figure 4.9: The phase diagrams of the models at $m_q = 50$ MeV with no explicit μ–dependence in the Polyakov potential. The solid line is the chiral transition and the dashed line the deconfinement transition. The dotted lines correspond to quark number densities of 1 fm^{-3} and 2 fm^{-3}. *Left*: PLSM with fermion vacuum contributions. *Right*: PNJL.

Including a explicit μ–dependence

A dependence on quark chemical potential can be included in the Polyakov potential. In [III] we used a formulation adopted from [42] with slight modifications discussed in [III] and in Chapter 3. The deconfinement transitions from the μ–dependent Polyakov potential can be seen in Figures 4.10 and 4.11. Comparison with Figures 4.8 and 4.9

reveals, as one would expect, that now the deconfinement transition temperature drops much more rapidly with increasing μ and thus is in better agreement with the chiral transition. However, as with the case without explicit chemical potential dependence in the Polyakov potential, Figures 4.10 and 4.11 illustrate that the deconfinement transition is independent from the amount of chiral symmetry breaking i.e. the bare quark mass, even when explicit μ–dependence is included in the potential. Thus the coincidence of the chiral and deconfinement transitions must be tuned into the models by hand. With the μ–dependent Polyakov potential this coincidence can be achieved for the whole lenght of the phase boundary, unlike in the case with no explicit μ–dependence in the Polyakov potential. Lattice calculations at finite μ indicating that the transition temperatures of chiral symmetry and deconfinement stay close to each other would provide a incentive to use the μ–dependent potential also in PLSM and PNJL type models.

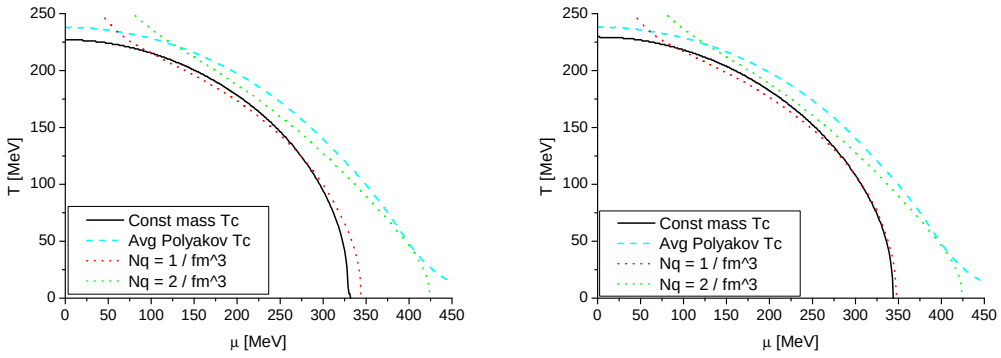

Figure 4.10: The phase diagrams of the models at the physical point $m_q \approx 5$ MeV with an explicit μ–dependence in the Polyakov potential. The solid line is the chiral transition and the dashed line the deconfinement transition. The dotted lines correspond to quark number densities of 1 fm^{-3} and 2 fm^{-3}. *Left*: PLSM with fermion vacuum contributions. *Right*: PNJL.

4.2.3 Quarkyonic matter

Recently it has been suggested in [70] that a new kind of matter could exist in the high μ low T region of the QCD phase diagram. This proposition is based on the 't Hooft large N_c limit of QCD. It is, however, unclear if $N_c = 3$ is large enough for the features of the 't Hooft limit to remain valid in QCD. Also a further complication arises from the fact that for QCD the large N_c limit is not unique. We have discussed these issues briefly in [III]. Also note a recent lattice study of possible quarkyonic matter [71]. Here, in this thesis, the possibility of examining the phase diagram for hints of quarkyonic matter withing effective model framework is discussed.

The authors of [70] suggest that the baryon density of the system could serve as an

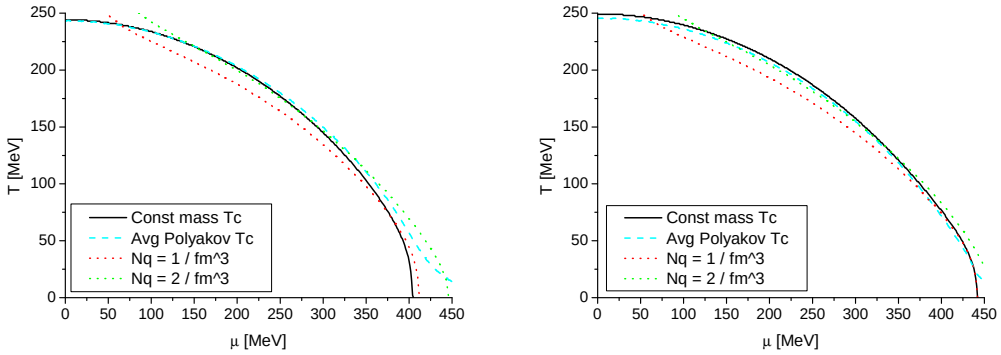

Figure 4.11: The phase diagrams of the models at $m_q = 50$ MeV with an explicit μ–dependence in the Polyakov potential. The solid line is the chiral transition and the dashed line the deconfinement transition. The dotted lines correspond to quark number densities of 1 fm^{-3} and 2 fm^{-3}. *Left*: PLSM with fermion vacuum contributions. *Right*: PNJL.

indicator for quarkyonic matter. Particularly a non–vanishing baryon density in the confined region of the phase diagram is suggested to be characteristic to the quarkyonic phase. In the PLSM and PNJL models the closest thing we have to probe the baryon density is quark number density n_q. If we consider low temperature where the system is confined i.e. $\ell, \ell^* \approx 0$, we get

$$n_q = \frac{\partial \Omega}{\partial \mu} = \frac{6}{\pi^2} \int_0^\infty p^2 dp \left[\frac{1}{1 + e^{3(E-\mu)}} - \frac{1}{1 + e^{3(E+\mu)}} \right], \tag{4.3}$$

from which we can see that thermal excitations near $T = 0$ are three quark states that are symmetric with respect to the $Z(3)$ symmetry i.e. baryons.

In the case with no μ–dependence in the Polyakov potential there is a rise in the value of the quark number density located near the chiral transition boundary when crossing to the chirally symmetric side as seen in Figure 4.12. At $T = 5$ MeV the magnitude of the rise is around 1 fm^{-3} with the relative increase being significant, since the absolute value of n_q is nearly zero in the chirally broken phase. Such a rise in the value makes it possible to argue that the quark number density indeed jumps from a (nearly) zero value to a non–zero one. As one goes to higher temperatures the behaviour of n_q becomes smoother and the transition to possible quarkyonic matter resembles more of a crossover.

One can also try to characterize the quarkyonic transition by assigning a value for n_q above which the system is considered to be in a quarkyonic phase. The problem here is that such a value is not unique. In Figures 4.8 and 4.9 two dotted lines are shown corresponding to values 1fm^{-3} and 2 fm^{-3} of n_q along with the deconfinement and chiral transition curves. If one estimates a baryon as a sphere with diameter $\sim$ 1.5 fm [72] then one could expect it to have a quark number density $\sim$ 2 fm^{-3}.

As a result, one should then consider having reached a phase with non–zero baryon density no later than when the average quark number density reaches $\sim 2\ \mathrm{fm}^{-3}$. This combined with the fact that the deconfinement transition line curves down very slowly and lies at high temperature, leaves significant room for quarkyonic matter to exist as pictured in [70].

If one then considers the case where the Polyakov loop potential depends explicitly on μ, the situation changes considerably. Figures 4.10 and 4.11 illustrate this. The most important, and obvious, difference is in the behaviour of the deconfinement transition line. It now follows the chiral transition line more closely, narrowing the window for a possible quarkyonic phase considerably. If we also keep in mind that when we implemented the μ–dependence to the Polyakov potential, we neglected effects from quark masses and the number of quark flavors. These, if taken into account, would lead to the deconfinement transition line being even lower than in Figures 4.10 and 4.11 and thus possibly closing the window for quarkyonic matter completely. The quark number densities are somewhat affected by the inclusion of μ–dependence to the Polyakov potential: The lines $n_q = 1\ \mathrm{fm}^{-3}$ and $n_q = 2\ \mathrm{fm}^{-3}$ are now generally closer together. This means that the n_q gradients have grown larger with the inclusion of the Polyakov loop μ–dependence, particularly at higher T and near the chiral transition. This can also be observed from Figure 4.12.

The conclusion about the possible existence of quarkyonic matter is then twofold: With a μ–independent Polyakov potential the window for quarkyonic matter is considerable while a μ–dependent potential leaves much less room for such matter to exist. Of course these conclusions are highly model dependent and our implementation of the μ–dependence is just one possibility to consider. Other approaches with similar results can be found for example in [44, 51, 52].

4.3 Adiabats

The isentropic evolution of a thermodynamic system with an equation of state that of the PLSM and PNJL models was studied in [I]. This study was motivated by claims that the hydrodynamic evolution of the system could exhibit a focusing behaviour that would take the system near the critical point from almost any initial condition. These claims have been advocated for in e.g. [73] which is in turn motivated by [74]. Given the success of ideal hydrodynamics in describing RHIC data, it is likely that the evolution of the plasma is isentropic. If this assumption is correct then the expansion of the system would follow the adiabats plotted in Figures 4.13 and 4.14 for the PLSM and PNJL models, respectively. However, the conclusion from these figures is that no focusing occurs in these models. Also there is no special behaviour near the critical points. A lattice calculation [75] shows similar results. Thus the conclusion is that the

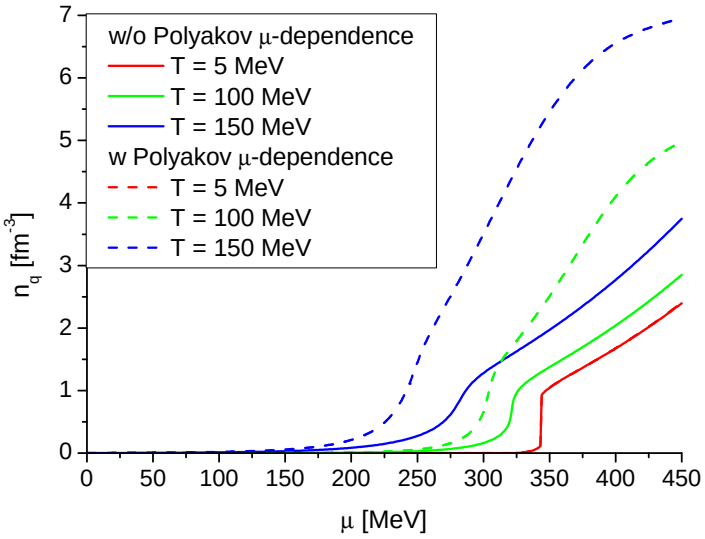

Figure 4.12: The quark number density n_q as a function of quark chemical potential μ for three temperatures $T = 5$ MeV $T = 100$ MeV and $T = 150$ MeV in the PNJL model. The solid lines correspond to the case where the Polyakov potential has no μ–dependence, while the dashed lines represent the case where the Polyakov potential depends explicitly on μ.

focusing behaviour observed in [74] is probably a feature of the particular equation of state used and not of the hydrodynamic approach in general.

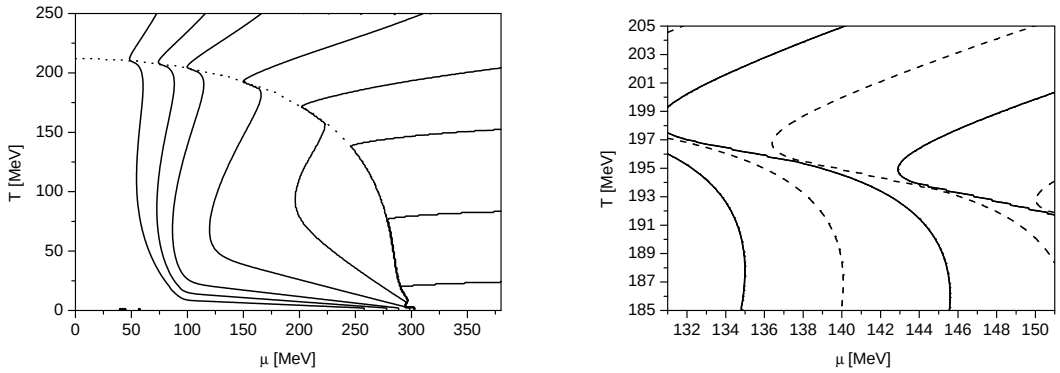

Figure 4.13: *Left Panel*: Constant S/N curves in the PLSM model. *Right Panel:* A close–up on the critical point at $(T_c, \mu_c) = (195, 141)$ MeV. Every second curve has been drawn with the dashed line to enhance readability.

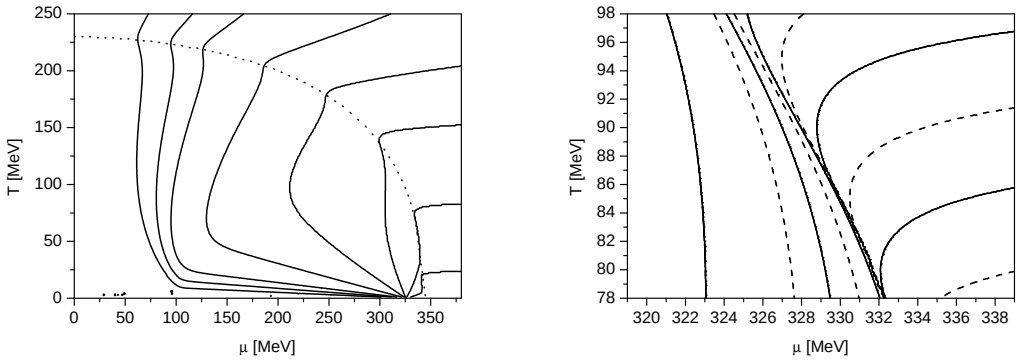

Figure 4.14: *Left Panel*: Constant S/N curves in the PNJL model. *Right Panel:* A close–up on the critical point at $(T_c, \mu_c) = (88, 329)$ MeV. Every second curve has been drawn with the dashed line to enhance readability.

5 Summary and outlook

In this thesis the thermodynamical properties of QCD were studied through two effective models, PLSM and PNJL. The models were constructed in a way that combined chiral dynamics (LSM and NJL) with the pure gauge sector. It was then found that such a combination describes, for example, the QCD pressure, obtained from pQCD and lattice calculations, better than the chiral models alone.

In this kind of a framework it is also possible to study the chiral and deconfinement transitions in a consistent setup and the results at zero chemical potential can be fitted to reproduce lattice QCD results. Then, unlike on the lattice, the extension to finite chemical potential is relatively easy. However, the results depend heavily on the model details. The critical point, for example, is quite differently located in the three cases, PLSM with and without fermion vacuum contributions and PNJL, studied in this thesis. Beyond mean field studies of the models, by other authors, have also suggested multiple critical points to be a possibility. Also the deconfinement transition can be implemented with or without a dependence on quark chemical potential. These cause a very different behaviour of the deconfinement transition in the (T, μ)–plane which, in turn, plays a vital role in determining the possibility of the so called quarkyonic phase in the QCD phase diagram. The window for quarkyonic matter was found to be significantly reduced with a μ–dependent gauge potential. Of course the way in which one includes the possible μ–dependence is also, along with the results, heavily model dependent.

Since the models incorporate degrees of freedom from two opposite limits of QCD, the chiral and pure gauge limits, the model dependence on the amount of explicit chiral symmetry breaking was also studied in order to establish how are the dynamics between the two sectors affected by this. This was done by controlling the bare quark mass in the models. The perhaps rather unsurprising result was that the deconfinement transition was not significantly altered when varying the bare quark mass. This is because the gauge potential in the models does not explicitly include the quark mass nor is the interaction connecting the two sectors able to mediate the effects to the pure gauge sector. In the future this could be improved by the using a gauge potential that depends explicitly on the quark mass. However, the chiral sector is, as expected, quite sensitive to the quark mass and the chiral transition line as well as the location of the critical point are affected. It was also found that the two different chiral approaches, LSM and NJL, result in qualitatively different behaviour when considering the location of the critical point as a function of quark mass. This is an interesting result since

in LSM the extension to unphysical quark masses is done via a lattice formula used to connect the physical observables, that serve as input to the model, in a consistent way. In the NJL the physical observables arise from the model and the only tunable input is the bare quark mass.

Overall the PLSM and PNJL type models seem to be flexible tools in exploring the QCD phase diagram and a number of different scenarios can be covered within the model framework. Unfortunately there is currently only a scarce amount of lattice data and practically no experimental information on which to judge the feasibility of these different scenarios. Some predictions, like the location of the critical point, are quite sensitive to model parameters and more information from lattice QCD or experiments is required to distinguish good parameter choices from bad ones. Also the coincidence of the chiral and deconfinement transitions is put by hand into these models and, if QCD indeed has a deeper connection between these transitions, a more robust mechanism of achieving this coincidence should be found.

Despite the success of the standard model we know that it is incomplete and there are many open questions to be answered, for example the origin of particle masses is still unresolved. In addition to describing QCD, the PLSM and PNJL type models could be used to describe physics beyond the standard model. Particularly technicolor scenarios, which greatly resemble QCD, could be studied with these models. The recent beginning of LHC experiments will hopefully shed light to many questions involving beyond standard model physics and in the spotlight are such theories as supersymmetry, technicolor and even string theory. But the LHC is expected to answer questions still open within the realm of the standard model, since now almost a hundred years after the discovery of the atomic nucleus and over 40 years after the birth of QCD there is still much to learn also about the strong interaction and the LHC heavy ion program and the ALICE (*A Large Ion Collider Experiment)* are designed with this in mind. However, the LHC will not tackle these questions alone: RHIC has been running for a decade with great success and will hopefully run for years to come providing valuable data on the properties of strongly interacting matter. Also by the end of the second decade of the millennium the CBM experiment will be running at the FAIR facility increasing our ability to probe the different phases of QCD. All in all the forthcoming decades will be an age of discovery beyond the standard model, but also within it.

References

[I] Topi Kähärä and Kimmo Tuominen. Degrees of freedom and the phase transitions of two flavor QCD. *Phys. Rev.*, D78:034015, 2008.

[II] Topi Kähärä and Kimmo Tuominen. Effective models of two-flavor QCD: from small towards large m_q. *Phys. Rev.*, D80:114022, 2009.

[III] Topi Kähärä and Kimmo Tuominen. Effective models of two-flavor QCD: finite μ and m_q-dependence. *Accepted for publication in Phys. Rev.*, D, 2010.

[1] Murray Gell-Mann. A Schematic Model of Baryons and Mesons. *Phys. Lett.*, 8:214–215, 1964.

[2] Leonard Susskind. Lattice Models of Quark Confinement at High Temperature. *Phys. Rev.*, D20:2610–2618, 1979.

[3] Daniel V Schroeder Michael E. Peskin. *An Introduction to Quantum Field Theory.* Wetview Press, 1995.

[4] E. S. Abers and B. W. Lee. Gauge Theories. *Phys. Rept.*, 9:1–141, 1973.

[5] Gerard 't Hooft. On the Phase Transition Towards Permanent Quark Confinement. *Nucl. Phys.*, B138:1, 1978.

[6] Alexander M. Polyakov. Thermal Properties of Gauge Fields and Quark Liberation. *Phys. Lett.*, B72:477–480, 1978.

[7] Gerard 't Hooft. A Property of Electric and Magnetic Flux in Nonabelian Gauge Theories. *Nucl. Phys.*, B153:141, 1979.

[8] Nathan Weiss. The Effective Potential for the Order Parameter of Gauge Theories at Finite Temperature. *Phys. Rev.*, D24:475, 1981.

[9] Larry D. McLerran and Benjamin Svetitsky. Quark Liberation at High Temperature: A Monte Carlo Study of SU(2) Gauge Theory. *Phys. Rev.*, D24:450, 1981.

[10] Nathan Weiss. The Wilson Line in Finite Temperature Gauge Theories. *Phys. Rev.*, D25:2667, 1982.

[11] Benjamin Svetitsky and Laurence G. Yaffe. Critical Behavior at Finite Temperature Confinement Transitions. *Nucl. Phys.*, B210:423, 1982.

[12] Benjamin Svetitsky. Symmetry Aspects of Finite Temperature Confinement Transitions. *Phys. Rept.*, 132:1–53, 1986.

[13] F. Karsch. SIMULATING THE QUARK - GLUON PLASMA ON THE LATTICE. *Adv. Ser. Direct. High Energy Phys.*, 6:61–115, 1990.

[14] Janos Polonyi. THE CONFINEMENT - DECONFINEMENT MECHANISM. *Adv. Ser. Direct. High Energy Phys.*, 6:1–60, 1990.

[15] A. V. Smilga. Aspects of chiral symmetry. 2000. hep-ph/0010049.

[16] Robert D. Pisarski. Notes on the deconfining phase transition. 2002.

[17] Joseph I. Kapusta. *Finite-temperature field theory.* Press Syndicate of the University of Cambridge, 1989.

[18] Frithjof Karsch. Lattice qcd at high temperature and density. *Lect. Notes Phys.*, 583:209–249, 2002.

[19] Y. Aoki, Z. Fodor, S. D. Katz, and K. K. Szabo. The QCD transition temperature: Results with physical masses in the continuum limit. *Phys. Lett.*, B643:46–54, 2006.

[20] Kenneth G. Wilson. CONFINEMENT OF QUARKS. *Phys. Rev.*, D10:2445–2459, 1974.

[21] A. Gocksch and Michael Ogilvie. FINITE TEMPERATURE DECONFINEMENT AND CHIRAL SYMMETRY RESTORATION AT STRONG COUPLING. *Phys. Rev.*, D31:877, 1985.

[22] J. B. Kogut, H. W. Wyld, F. Karsch, and D. K. Sinclair. FIRST ORDER CHIRAL PHASE TRANSITION IN LATTICE QCD. *Phys. Lett.*, B188:353, 1987.

[23] Y. Aoki et al. The QCD transition temperature: results with physical masses in the continuum limit II. *JHEP*, 06:088, 2009.

[24] Christian Schmidt. Lattice QCD at finite density. *PoS*, LAT2006:021, 2006.

[25] Frithjof Karsch. Lattice results on QCD at high temperature and non-zero baryon number density. *Prog. Part. Nucl. Phys.*, 62:503–511, 2009.

[26] G. Boyd et al. Thermodynamics of SU(3) Lattice Gauge Theory. *Nucl. Phys.*, B469:419–444, 1996.

[27] Ting-Wai Chiu and Tung-Han Hsieh. Light quark masses, chiral condensate and quark-gluon condensate in quenched lattice QCD with exact chiral symmetry. *Nucl. Phys.*, B673:217–237, 2003.

[28] Teiji Kunihiro et al. Scalar mesons in lattice QCD. *Phys. Rev.*, D70:034504, 2004.

[29] Massimiliano Procura, Thomas R. Hemmert, and Wolfram Weise. Nucleon mass, sigma term and lattice QCD. *Phys. Rev.*, D69:034505, 2004.

[30] A. Ipp, A. Rebhan, and A. Vuorinen. Perturbative QCD at non-zero chemical potential: Comparison with the large-N(f) limit and apparent convergence. *Phys. Rev.*, D69:077901, 2004.

[31] O. Scavenius, A. Mocsy, I. N. Mishustin, and D. H. Rischke. Chiral phase transition within effective models with constituent quarks. *Phys. Rev.*, C64:045202, 2001.

[32] Dirk Roder, Jorg Ruppert, and Dirk H. Rischke. Chiral symmetry restoration in linear sigma models with different numbers of quark flavors. *Phys. Rev.*, D68:016003, 2003.

[33] Kenji Fukushima. Chiral effective model with the Polyakov loop. *Phys. Lett.*, B591:277–284, 2004.

[34] A. Mocsy, I. N. Mishustin, and P. J. Ellis. Role of fluctuations in the linear sigma model with quarks. *Phys. Rev.*, C70:015204, 2004.

[35] Claudia Ratti, Michael A. Thaler, and Wolfram Weise. Phases of QCD: Lattice thermodynamics and a field theoretical model. *Phys. Rev.*, D73:014019, 2006.

[36] H. Hansen et al. Mesonic correlation functions at finite temperature and density in the Nambu-Jona-Lasinio model with a Polyakov loop. *Phys. Rev.*, D75:065004, 2007.

[37] C. Ratti, Simon Roessner, M. A. Thaler, and W. Weise. Thermodynamics of the PNJL model. *Eur. Phys. J.*, C49:213–217, 2007.

[38] Simon Roessner, Claudia Ratti, and W. Weise. Polyakov loop, diquarks and the two-flavour phase diagram. *Phys. Rev.*, D75:034007, 2007.

[39] C. Sasaki, B. Friman, and K. Redlich. Susceptibilities and the phase structure of a chiral model with Polyakov loops. *Phys. Rev.*, D75:074013, 2007.

[40] Claudia Ratti, Simon Roessner, and Wolfram Weise. Quark number susceptibilities: Lattice QCD versus PNJL model. *Phys. Lett.*, B649:57–60, 2007.

[41] Simon Roessner, T. Hell, C. Ratti, and W. Weise. The chiral and deconfinement crossover transitions: PNJL model beyond mean field. *Nucl. Phys.*, A814:118–143, 2008.

[42] Bernd-Jochen Schaefer, Jan M. Pawlowski, and Jochen Wambach. The Phase Structure of the Polyakov–Quark-Meson Model. *Phys. Rev.*, D76:074023, 2007.

[43] H. Abuki, R. Anglani, R. Gatto, M. Pellicoro, and M. Ruggieri. The fate of pion condensation in quark matter: from the chiral to the real world. *Phys. Rev.*, D79:034032, 2009.

[44] H. Abuki, R. Anglani, R. Gatto, G. Nardulli, and M. Ruggieri. Chiral crossover, deconfinement and quarkyonic matter within a Nambu-Jona Lasinio model with the Polyakov loop. *Phys. Rev.*, D78:034034, 2008.

[45] Kenji Fukushima. Phase diagrams in the three-flavor Nambu–Jona-Lasinio model with the Polyakov loop. *Phys. Rev.*, D77:114028, 2008.

[46] Tomasz L. Partyka and Mariusz Sadzikowski. Phase diagram of the non-uniform chiral condensate in different regularization schemes at T=0. *J. Phys.*, G36:025004, 2009.

[47] Bernd-Jochen Schaefer and Mathias Wagner. The three-flavor chiral phase structure in hot and dense QCD matter. *Phys. Rev.*, D79:014018, 2009.

[48] Pedro Costa, H. Hansen, M. C. Ruivo, and C. A. de Sousa. How parameters and regularization affect the PNJL model phase diagram and thermodynamic quantities. *Phys. Rev.*, D81:016007, 2010.

[49] Kenji Fukushima. Isentropic thermodynamics in the PNJL model. *Phys. Rev.*, D79:074015, 2009.

[50] Lorenzo Ferroni, Volker Koch, and Marcus B. Pinto. Multiple Critical Points in Effective Quark Models. 2010.

[51] Tina Katharina Herbst, Jan M. Pawlowski, and Bernd-Jochen Schaefer. The phase structure of the Polyakov–quark-meson model beyond mean field. 2010.

[52] G. Marko and Zs. Szep. Influence of the Polyakov loop on the chiral phase transition in the two flavor chiral quark model. 2010.

[53] J. Moreira, B. Hiller, A. A. Osipov, and A. H. Blin. The phase diagram in the SU(3) Nambu-Jona-Lasinio model with 't Hooft and eight-quark interactions. *AIP Conf. Proc.*, 1257:676–680, 2010.

[54] Leticia F. Palhares and Eduardo S. Fraga. Droplets in the cold and dense linear sigma model with quarks. 2010.

[55] M. C. Ruivo, Pedro Costa, H. Hansen, and C. A. de Sousa. Exploring the role of model parameters and regularization procedures in the thermodynamics of the PNJL model. *AIP Conf. Proc.*, 1257:681–685, 2010.

[56] V. Skokov, B. Friman, E. Nakano, K. Redlich, and B. J. Schaefer. Vacuum fluctuations and the thermodynamics of chiral models. *Phys. Rev.*, D82:034029, 2010.

[57] V. Skokov, B. Friman, and K. Redlich. The renormalization group and quark number fluctuations in the Polyakov loop extended quark-meson model at finite baryon density. 2010.

[58] Yoichiro Nambu and G. Jona-Lasinio. Dynamical model of elementary particles based on an analogy with superconductivity. i. *Phys. Rev.*, 122:345–358, 1961.

[59] S. P. Klevansky. The Nambu-Jona-Lasinio model of quantum chromodynamics. *Rev. Mod. Phys.*, 64:649–708, 1992.

[60] Gerard 't Hooft. Topology of the Gauge Condition and New Confinement Phases in Nonabelian Gauge Theories. *Nucl. Phys.*, B190:455, 1981.

[61] M. Asakawa and K. Yazaki. CHIRAL RESTORATION AT FINITE DENSITY AND TEMPERATURE. *Nucl. Phys.*, A504:668–684, 1989.

[62] Stephen R. Sharpe. Quenched chiral logarithms. *Phys. Rev.*, D46:3146–3168, 1992.

[63] F. Karsch, E. Laermann, and A. Peikert. Quark mass and flavor dependence of the QCD phase transition. *Nucl. Phys.*, B605:579–599, 2001.

[64] Mikko Laine and York Schroder. Quark mass thresholds in QCD thermodynamics. *Phys. Rev.*, D73:085009, 2006.

[65] We thank Mikko Laine for providing us with the numerical results for the two–flavor case.

[66] F. Karsch, K. Redlich, and A. Tawfik. Thermodynamics at non-zero baryon number density: A comparison of lattice and hadron resonance gas model calculations. *Phys. Lett.*, B571:67–74, 2003.

[67] E. Nakano, B. J. Schaefer, B. Stokic, B. Friman, and K. Redlich. Fluctuations and isentropes near the chiral critical endpoint. *Phys. Lett.*, B682:401–407, 2010.

[68] Yoshitaka Hatta and Takashi Ikeda. Universality, the QCD critical / tricritical point and the quark number susceptibility. *Phys. Rev.*, D67:014028, 2003.

[69] E. Scott Bowman and Joseph I. Kapusta. Critical Points in the Linear Sigma Model with Quarks. *Phys. Rev.*, C79:015202, 2009.

[70] Larry McLerran and Robert D. Pisarski. Phases of Cold, Dense Quarks at Large N_c. *Nucl. Phys.*, A796:83–100, 2007.

[71] Simon Hands, Seyong Kim, and Jon-Ivar Skullerud. A Quarkyonic Phase in Dense Two Color Matter? *Phys. Rev.*, D81:091502, 2010.

[72] Claude Amsler et al. Review of particle physics. *Phys. Lett.*, B667:1, 2008.

[73] Roy A. Lacey et al. Has the QCD critical point been signaled by observations at RHIC? *Phys. Rev. Lett.*, 98:092301, 2007.

[74] Chiho Nonaka and Masayuki Asakawa. Hydrodynamical evolution near the QCD critical end point. *Phys. Rev.*, C71:044904, 2005.

[75] S. Ejiri, F. Karsch, E. Laermann, and C. Schmidt. The isentropic equation of state of 2-flavor QCD. *Phys. Rev.*, D73:054506, 2006.